Southern Plains Transportation Center
CYCLE 1

# FINAL REPORT

2023–2024

USDOT BIL Regional UTC
Region 6

---

## Advanced Concrete Materials for Rapid Infrastructure Repair and Rehabilitation

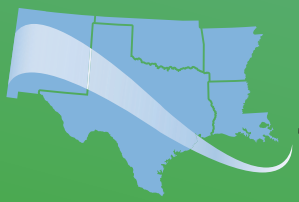

SOUTHERN PLAINS
TRANSPORTATION CENTER

# Disclaimer

The contents of this report reflect the views of the authors, who are responsible for the facts and accuracy of the information presented herein. This document is disseminated under the sponsorship of the Department of Transportation University Transportation Centers Program, in the interest of information exchange. The U.S. Government assumes no liability for the contents or use thereof.

# Technical Report Documentation Page

| | | |
|---|---|---|
| 1. Report No.<br>CY1-UARK-LSU-01 | 2. Government Accession No.[Leave blank] | 3. Recipient's Catalog No.<br>[Leave blank] |
| 4. Title and Subtitle<br>Advanced Concrete Materials for Rapid Infrastructure Repair and Rehabilitation | | 5. Report Date<br>January, 2025 |
| | | 6. Performing Organization Code [Code] |
| 7. Author(s)<br>Cameron Murray 0000-0002-7392-7849 https://orcid.org/0000-0002-7392-7849<br>Hassan Noorvand 0000-0002-4798-2051 https://orcid.org/0000-0002-4798-2051<br>Elizabeth Poblete 0000-0002-5680-306X https://orcid.org/0000-0002-5680-306X<br>Adriana A. Alvarado 0000-0002-7943-6477 https://orcid.org/0000-0002-7943-6477 | | 8. Performing Organization Report No.<br>[Report No.] |
| 9. Performing Organization Name and Address<br>University of Arkansas<br>1 University of Arkansas<br>Fayetteville, AR 72701<br><br>Louisiana State University<br>3315A Patrick F. Taylor Hall<br>OA ton Rouge, LA 70803 | | 10. Work Unit No. (TRAIS)<br>[Leave blank] |
| | | 11. Contract or Grant No.<br>69A3552348306 |
| 12. Sponsoring Agency Name and Address<br>Southern Plains Transportation Center<br>202 West Boyd St., Room 213B<br>The University of Oklahoma<br>Norman, OK 73019 | | 13. Type of Report and Period Covered<br>[Final Report (September 2023- December 2024)] |
| | | 14. Sponsoring Agency Code [Leave blank] |

15. Supplementary Notes
Conducted in cooperation with the U.S. Department of Transportation as a part of University Transportation Center (UTC) program.

16. Abstract
This project demonstrates the use of belitic calcium sulfoaluminate (BCSA) cement in engineered cementitious composites (ECC) and measures the corrosion performance of BCSA cement concrete using ASTM G109. BCSA cement is a fast setting, fast strength gain, low shrinkage cement which can be mixed similarly to Portland cement (PC) but has significantly different performance. For infrastructure projects, demonstrating the properties of BCSA ECC could lead to its greater implementation in bridges and pavements while reducing impacts. One important consideration in infrastructure made with reinforced concrete is the protection of the embedded rebar from corrosion. ASTM G109 exposes reinforced concrete to a chloride solution and determines when corrosion of the embedded rebar initiates. In this study, BCSA cement concrete was compared to PC and several variables were altered to attempt to modify or improve the corrosion resistance of the BCSA mixtures. BCSA presented a good alternative or supplement to PC in ECC. BCSA cement improved the crack width of ECC and improved early age strength. In terms of corrosion, rebar in BCSA cement concrete samples was generally more prone to corrosion than in PC, but the mix design and preparation of the BCSA cement concrete can be altered to significantly improve its corrosion behavior.

| | |
|---|---|
| 17. Key Words<br>Engineered cementitious composite, cement, corrosion, concrete, calcium sulfoaluminate | 18. Distribution Statement<br>No restrictions. This publication is available at www.sptc.org and from the NTIS. |

| | | | |
|---|---|---|---|
| 19. Security Classification (of this report) Unclassified | 20. Security Classification (of this page) Unclassified | 21. No. of Pages<br>81 | 22. Price<br>N/A |

Form DOT F 1700.7 (8-72) Reproduction of completed page authorized

# ADVANCED CONCRETE MATERIALS FOR RAPID INFRASTRUCTURE REPAIR AND REHABILITATION

FINAL REPORT

SPTC Project Number: CY1-UARK-LSU-01

Submitted by
Dr. Cameron D Murray (PI)
Dr. Hassan Noorvand (PI)
Elizabeth S.M. Poblete (Graduate Student)
Adriana A. Alvarado-Ramirez (Graduate Student)
Department of Civil Engineering
University of Arkansas
Bert S. Turner Department of Construction Management-College of Engineering
Louisiana State University

Prepared for
Southern Plains Transportation Center
The University of Oklahoma
Norman, OK

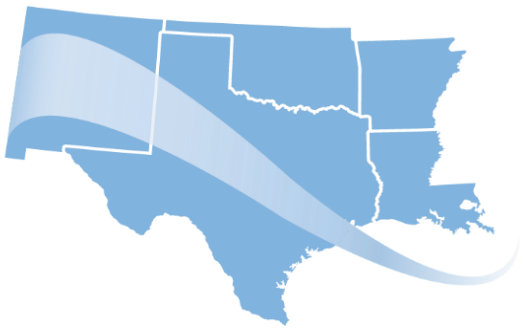

SOUTHERN PLAINS
TRANSPORTATION CENTER

January 2025

# Acknowledgments

The authors would like to acknowledge the financial support from the Southern Plains Transportation Center through grant No. CY1-LSU-2.2 as well as the support of the Louisiana Transportation Research Center (LTRC). Authors acknowledge the material donations of Eco Materials Technologies and CTS Cement Manufacturing Corporation.

**Table of Contents**

# List of Tables

# List of Figures

# List of Equations

# List of Abbreviations and Acronyms

| | |
|---|---|
| ACI | American Concrete Institute |
| $Al_2O_3$ | Aluminium oxide |
| ASTM | American Society for Testing and Materials |
| BCSA | Belitic calcium sulfoaluminate |
| C | Coulombs |
| C4A3Ŝ | Ye'elimite or $Ca_4(AlO_2)_6(SO_4)$ |
| $C_2S$ | Dicalcium silicate |
| $C_3S$ | Tricalcium silicate |
| CEP | Engagement and Participation |
| C-S-H | Calcium silicate hydrate |
| CH | Calcium hydroxide |
| cm | Centimeter |
| $CO_2$ | Carbon dioxide |
| ECC | Engineered Cementitious Composite |
| FA | Fly ash |
| $Fe_2O_3$ | Iron (III) oxide |
| fc | Compressive strength |
| FRC | Fiber-reinforced concrete |
| HRWR | High-range water reducer |
| in. | Inch |
| kN | Kilonewton |
| lbf | Pound-force |
| LOI | Loss on ignition |
| mm | Millimeter |
| NDT | Non-Destructive Testing |
| OA | Oak Grove Pozzolan Coal Ash |
| PC | Type I Portland Cement |
| PE | Ultra-high molecular weight polyethylene |
| PSH | Pseudo-strain-hardening |
| RPM | Revolutions per minute |
| SCMs | Supplementary cementitious materials |
| SEM | Scanning electron microscopy |
| $SiO_2$ | Silicon dioxide |
| $SO_3$ | Sulfur trioxide |
| TC | Total corrosion |
| UPV | Ultrasonic pulse velocity |
| w/cm | Water to cementitious materials ratio |
| XRD | X-ray diffraction |
| XRF | X-ray fluorescence |

# Executive Summary

This report explores innovative concrete materials to address the growing demands of infrastructure maintenance and responsibility. Specifically, it investigates the potential of belitic calcium sulfoaluminate (BCSA) cement for use in engineered cementitious composites (ECCs) and the corrosion resistance of concrete made with BCSA cement. BCSA cement has emerged as a promising material due to its reduced impacts, rapid setting properties, and lower shrinkage compared to Portland cement (PC). These attributes make it particularly suitable for time-sensitive repair applications, where efficiency and durability are paramount. ECCs, renowned for their exceptional ductility, strain-hardening capabilities, and superior mechanical performance, offer significant advantages in enhancing the durability and extending the service life of transportation infrastructure. By combining BCSA cement with ECC technology, this research aims to deliver high-performance solutions that align with modern construction and condition demands. An ECC made with BCSA cement has yet to be demonstrated. In this report, the proportioning and testing of a BCSA cement ECC is described.

Additionally, BCSA cement has significantly different microstructural properties compared with Portland cement. This leads to open questions about its long-term durability. One durability issue is the protection of steel rebar from corrosion. This report details a durability study which subjects BCSA cement concrete to high-chloride exposure and determines the factors (cover depth, w/c, curing time, additives) that lead to improved corrosion performance compared to a typical PC mixture.

The results of this study show that BCSA based ECC can achieve similar flow results to PC based ECC. Using BCSA in ECC also accelerates the setting time and strength gain of ECC. Longer-term strengths are sometimes better with PC based ECC, but the use of BCSA cement improved crack widths and the engagement of fiber reinforcement. The corrosion performance of BCSA cement was worse than the companion PC samples when using the standard corrosion test method procedures. However, if the BCSA cement is allowed to reach a greater level of maturity through a longer moist curing period, the corrosion performance of the BCSA cement concrete improved. Additionally, corrosion performance of BCSA cement concrete can be improved through reducing the w/c, increasing cover depth, and the use of sealers. If BCSA cement concrete is used in conditions where there is significant exposure to chlorides, these measures can make the corrosion performance better than the standard PC mixture tested here.

# Chapter 1. Introduction

The construction industry heavily relies on cement-based materials, particularly concrete, for infrastructure production (Marsh et al. 2022). With the increasing global demand for concrete and cement, the need for innovative alternatives is becoming critical (Almutairi et al. 2021; Olsson et al. 2023). Aging infrastructure in developed nations has created a growing demand for repair, rehabilitation, and retrofitting. In the United States alone, annual costs for these efforts exceed $20 billion (Gardner et al., 2018; Zhou et al., 2016). Many structural failures stem from durability issues such as cracking, brittleness, and steel corrosion (Mehta et al., 1982), highlighting the need for advanced materials that address these limitations while offering improved hardened concrete characteristics such as compressive strength, tensile strength, and ductility.

Engineered Cementitious Composite (ECC), a pseudo strain-hardening material developed by Victor C. Li in the late 1990s, is a promising solution to these challenges. ECCs incorporate supplementary cementitious materials (SCMs), such as fly ash and silica fume, which reduce impacts, material costs, and the reliance on natural resources (Almutairi et al., 2021). With tensile strain capacities exceeding 2%, ECCs mitigate the brittleness of conventional concrete, providing superior durability and resilience in structural applications (Li, 2019). Their performance is based on a micromechanical design that optimizes fiber-matrix interactions, allowing the material to resist multiple tension-induced cracks and preventing catastrophic failures (Ding et al., 2018).

A common failure mechanism of concrete infrastructure, both prestressed and reinforced, is the corrosion of embedded steel (Mehta et al., 2006; Coppola et al., 2022). Corrosion of embedded steel can occur through two main pathways: chloride ion penetration and carbonation of concrete. Concrete structures exposed to marine conditions or de-icing salts are particularly at risk for corrosion due to their exposure to chloride ions. Carbonation can occur when hydration products interact with the atmosphere causing a carbonation reaction (Gastaldi et al., 2018). The products of the carbonation reaction are acidic, which lowers the pore solution pH from extremely basic (12.5-13.5) towards neutral, enhancing the likelihood of reinforcing steel corrosion (Mehta et al., 2006).

Among the alternatives to Portland cement (PC), belitic calcium sulfoaluminate (BCSA) cement is a particularly promising binder. The production of BCSA cement emits less and requires 25–60% less energy to produce compared to PC due to its lower kiln temperature requirements (Bescher et al., 2018; Deo et al., 2023; Zivica et al., 2014). In addition to these benefits, BCSA cement offers rapid setting times, increased early age compressive strength, good durability, and excellent dimensional stability, making it suitable for high-performance applications (Chen et al., 2012; Winnefeld et al., 2010). Rapid setting times and high early age strength can also increase the rate of construction. These properties make them an ideal candidate for rapidly replacing or repairing critical transportation infrastructure.

In addition, ECCs with superior ductility and mechanical strength have been proposed as a promising material alternative to extend the durability and service life of infrastructure. However, Portland cement based ECC typically requires a high cement content, leading to challenges such as autogenous shrinkage.

Alternative cements, including BCSA cement, were approved for use in structural concrete applications for the first time by American Concrete Institute (ACI) 318-19: Building Code Requirements for Structural Concrete. Approval for alternative cement usage may be granted given the availability of test data proving that concrete made with the alternative cement meets the structural, durability, and fire performance requirements of PC concrete (ACI Committee 318, 2019). Structural performance requirements may refer to hardened properties such as compressive strength ($f_c$), tensile strength, modulus of rupture or flexural strength, modulus of

elasticity and others. Durability performance requirements may refer to carbonation and corrosion protection, resistance to chemical attacks, freeze/thaw resistance, and others.

BCSA cement concrete may be a suitable alternative to PC concrete for rapid construction of structures or for use in ECC given its rapid hardening, increased early age compressive strength, and dimensional stability discussed above. But research is still required to prove that BCSA cement concrete meets the performance requirements as described by ACI 318-19 (ACI Committee 318, 2019) and that it can achieve similar high-performance as PC in ECC applications.

## Objectives and Scope

Despite the potential benefits of BCSA cement, its integration into ECCs has not been thoroughly explored. Although some studies have assessed the impact of BCSA in ECC formulations that include other minerals like gypsum; the effects of substituting Portland cement partially or fully with BCSA cement alone have not been sufficiently investigated (Gou et al., 2024; Lv et al., 2020). This research gap limits the broader implementation of BCSA based ECC in the construction industry. This study aims to address the existing knowledge gap by developing BCSA-enhanced ECC materials for infrastructure applications. Specifically, the objective of this study is to assess the impact of BCSA cement on ECC performance by partially or fully replacing PC. Additionally, the influence of Oak Grove Pozzolan Coal Ash (OA) on ECC properties was evaluated at two replacement levels (55% and 70%) under PC replacement conditions.

Although construction of infrastructure elements containing BCSA cement can decrease impacts and cost as a result of reduced construction time, there is a research gap surrounding its use in reinforced concrete. This research gap was identified in ACI 318-19 and questions about long-term durability must be answered to facilitate its broader use. Some previous research on BCSA cement concrete has revealed potentially reduced durability performance compared to PC concrete (Coppola et al., 2020; Duan et al., 2013; Zhang et al., 2005; Quillin, 2001; Gastaldi et al., 2018). This study aims to establish how protection of reinforcement from corrosion can be improved in BCSA cement concrete through varying w/cm, curing time, cover depth, and protective measures.

This report presents the findings and insights from the research, contributing to the advancement of practices in infrastructure management. By emphasizing innovative material development, the study provides actionable solutions to meet the increasing demand for resilient infrastructure.

# Chapter 2. Literature Review

## Cement

Cement is a versatile binder that, when mixed with water, undergoes a chemical reaction to harden and develop strength, making it a widely used material in construction (ASTM, 2024b). It is renowned for its ability to bond aggregates and other materials. Among its various types, Portland Cement Type I stand out for their characteristics and broad applications (ASTM, 2024a).

### Type I/II PC

Type I/II PC, commonly known as "general-purpose cement," is the most widely used type of PC It is manufactured from a mixture of limestone, clay, and other materials that are heated in a kiln to approximately 1450°C, forming a clinker, which is then finely ground into a powder (Aïtcin, 2016). When mixed with water, Type I/II PC undergoes a hydration reaction where the primary compounds—tricalcium silicate ($C_3S$) and dicalcium silicate ($C_2S$, belite)—react with water to form calcium silicate hydrate (C-S-H) and calcium hydroxide (CH) (Lewis et al., 2003).

This reaction is responsible for the hardening and strength development of the cement. Type I/II PC achieves a balanced setting time and consistent strength gain, making it suitable for a wide range of applications, such as buildings, bridges, and pavements. Its slower hydration rate compared to some other types makes it ideal for projects requiring steady strength gain over time, reducing the risk of thermal cracking in mass concrete structures (Bye, 1999; Lewis et al., 2003).

### BCSA Cement

Calcium sufloaluminate (CSA) cements are the family of alternative cements to which BCSA belongs. Alternative cements are defined by the ACI as inorganic, hydraulic cements other than PC or blends of PC and other materials.

In contrast to PC, BCSA cement offers an alternative by addressing the impact of traditional cement production. BCSA cement is fast hardening cement produced at a lower kiln temperature of around 1250°C (Bescher et al., 2018), significantly reducing energy consumption. Unlike Type I/II PC, BCSA cement achieves its strength through a hydration process involving its primary components, belite and ye'elimite ($Ca_4(AlO_2)_6(SO_4)$ or C4A3$\hat{S}$). This reaction generates ettringite and other phases that contribute to rapid setting, high early strength, excellent dimensional stability, and good durability properties against many exposure factors (Acarturk et al., 2023; Deo et al., 2023).

While Type I/II PC remains the standard choice for general-purpose construction due to its reliability and versatility (Aïtcin, 2016), BCSA cement's production process and unique hydration mechanisms make it an increasingly popular option (Deo et al., 2023). The complementary characteristics of these two cements highlight their respective strengths: Type I/II PC for cost effectiveness and its long track record of performance, and BCSA cement for rapid construction and reduced impacts (Deo et al., 2023; Aïtcin, 2016).

Since BCSA cement concrete is rapid hardening, it may not be practical to estimate early age in-situ hardened properties with traditional methods such as casting companion cylinders, allowing them to cure in ambient conditions, and transporting them to a lab for testing. Therefore, non-destructive methods for estimating $f_c$ must be established. ACI 228.1R-19: Report on Methods for Estimating In-Place Concrete Strength considers ultrasonic pulse velocity (UPV) as a possible method for estimating $f_c$ if a $f_c$-UPV relationship has been established and notes that the relationship between $f_c$ and UPV is highly nonlinear (ACI Committee 228, 2019). Previous

research concluded that the relationship between $f_c$ anad UPV may be defined by an equation in the form of Equation 1 (Mohammed et al., 2016).

$$f_c = A * e^{B*UPV}$$

**Equation 1**

where,

$f_c$=compressive strength

A=coefficient relating to aggregate type and sand/aggregate ratio

B=rate of change of compressive strength

UPV=measured ultrasonic pulse velocity

## Concrete

While Type I/II PC and BCSA cement each offer distinct advantages in terms of performance, their effectiveness in concrete applications must also account for the inherent limitations of concrete as a material. Concrete, a composite material made by mixing cement, aggregates, and water, is renowned for its compressive strength, durability, and versatility (Lewis et al., 2003). However, it has inherent weaknesses that impact its long-term performance, particularly its low tensile strength and limited strain capacity (El Maaddawy et al., 2005; Li, 2019). These deficiencies make concrete prone to cracking under loads (El Maaddawy et al., 2005). Cracks compromise the structural integrity of concrete, reducing its ability to carry loads effectively (El Maaddawy et al., 2005; Li, 2019). Additionally, cracks allow water and harmful chemicals to penetrate, accelerating deterioration through mechanisms like freeze-thaw cycles or corrosion of embedded steel reinforcement (S et al., 2023; Luo et al., 2022; El Maaddawy et al., 2005). Addressing these challenges is crucial for improving the longevity and durability of concrete pavements and other infrastructure (S et al., 2023).

## ECC

To overcome the limitations of traditional concrete, advanced materials such as ECC, often referred to as "bendable concrete," have been developed (Ding et al., 2018). ECC incorporates fiber reinforcement, specialized admixtures, and optimized mix designs to dramatically enhance tensile strength and strain capacity. Unlike traditional concrete, ECC forms tightly controlled micro-cracks under tensile stress, allowing it to withstand significant deformation without structural failure (Li, 2019).

ECC is a type of fiber-reinforced concrete (FRC), as it contains fiber in a cementitious matrix. ECC demonstrates a unique behavior resembling that of ductile metals, known as pseudo strain-hardening, greater strain deformation as the fibers help bridge cracks. This means that as strain increases, ECC continues to carry and even increase stress, forming controlled micro-cracks instead of failing, significantly enhancing its durability. In contrast, in Figure 1, FRC shows exhibits a tension-softening behavior after the appearance of a crack that continues to widen as the load bearing capacity decreases under tensile loading. Furthermore, traditional concrete exhibits brittle failure, abruptly breaking after minimal strain deformation due to its low tensile strength and strain capacity. In contrast, the strain capacity of ECC is typically over 2% or 200 times that of normal concrete or FRC (Li, 2019; Fischer et al., 2003).

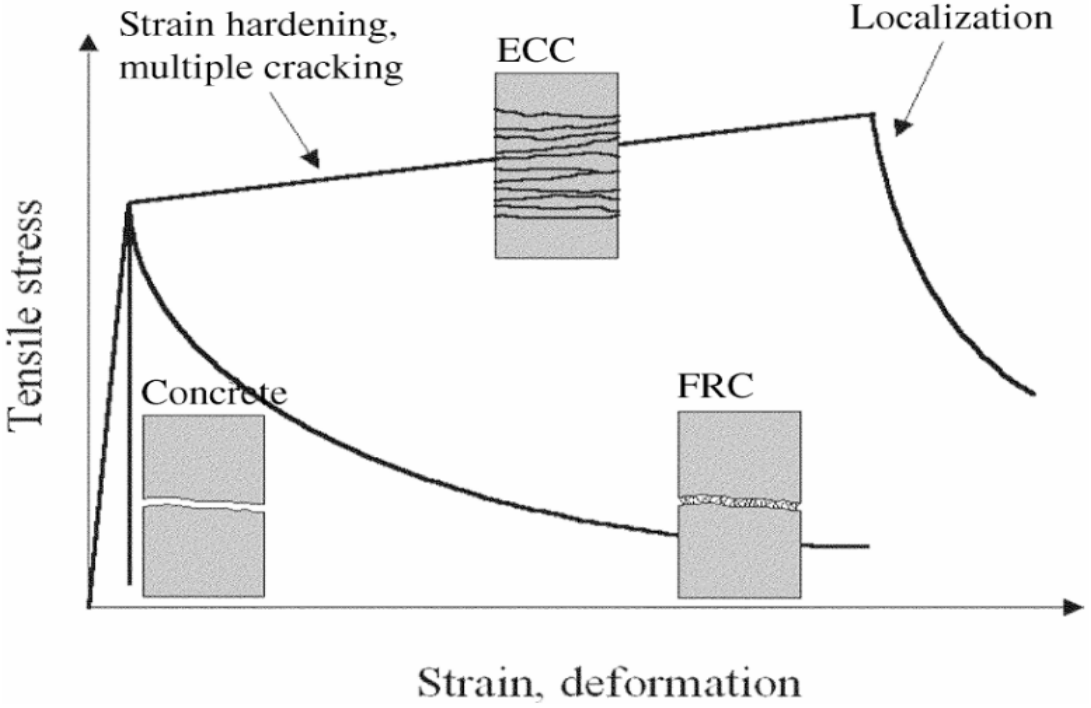


**Figure 1. Stress-strain behavior comparison between concrete, FRC, and ECC in tensile load (Fischer et al., 2003).**

Unlike traditional concrete, which is brittle and has low tensile strength and strain capacity, ECC can undergo significant deformation without cracking or failing. This is achieved through a carefully engineered mix that includes fine aggregates, specialized admixtures, and a low volume fraction of short, discontinuous fibers—often made from materials like polyvinyl alcohol (PVA) (Noorvand et al., 2019; Gabriel A. Arce et al., 2021; Noorvand et al., 2022). The key characteristic of ECC is its ability to form numerous tight micro-cracks, aided by the bonding between the matrix and the fiber, rather than a few wide cracks when subjected to tensile loads. These micro-cracks are typically less than 100 micrometers wide, which prevents the ingress of harmful substances like water and chlorides, thereby enhancing the material's durability. The controlled cracking behavior allows ECC to maintain its structural integrity and load-carrying capacity even after extensive deformation (Subedi et al., 2021; Li, n.d.). ECC's enhanced tensile properties and strain capacity make it particularly suitable for applications where durability and longevity are critical, such as in pavements, bridges, and seismic-resistant structures. By addressing the inherent weaknesses of conventional concrete, ECC contributes to the development of more resilient infrastructure (Ding et al., 2018; Li, 2019; Ding et al., 2022).

Li, Li, and Leung, along with their collaborators, established the theoretical framework that laid the groundwork for the invention of ECCs in the nineties. This framework is primarily built on micromechanics and fracture mechanics (Subedi et al., 2021; Li, n.d.). At the core of this framework are two key requirements for ECCs to display their characteristic pseudo-strain-hardening (PSH) behavior: the strength criterion and the energy criterion. The strength criterion, expressed in Equation 2, dictates that the maximum fiber-bridging capacity ($\sigma_0$) must surpass the first-cracking strength of the matrix ($\sigma_{fc}$) across any potential crack plane as displayed in Figure 2(Gabriel Arce et al., 2019).

$$\sigma_0 \geq \sigma_{fc}$$

**Equation 2**

Where,

$\sigma_0 =$ Maximum fiber-bridging capacity;

$\sigma_{fc} =$ First-cracking strength.

Conversely, the energy criterion, expressed at Equation 3, necessitates that the complementary energy $(J_b')$ obtained from the $\sigma(\delta)$ stress-displacement relation be greater than the crack-tip matrix toughness $(J_{tip})$ to guarantee that multiple steady-state cracks occur in the composite.

$$J_b' \equiv \sigma_0\delta_0 - \int_0^{\delta_0} \sigma(\delta)d\delta \geq J_{tip} \equiv \sigma_{ss}\delta_{ss} - \int_0^{\delta_{ss}} \sigma(\delta)d\delta$$

**Equation 3**

Where,

$J_b' =$ Complementary energy of the fiber-bridging relation

$J_{tip} =$ Crack tip matrix toughness

$\delta_0 =$ Crack opening corresponding to $\sigma_0$

$\sigma(\delta) =$ Complete stress vs. crack-opening relationship of the bridging fibers

$\sigma_{ss} =$ Steady-state tensile stress

$\delta_{ss} =$ Steady-state crack opening

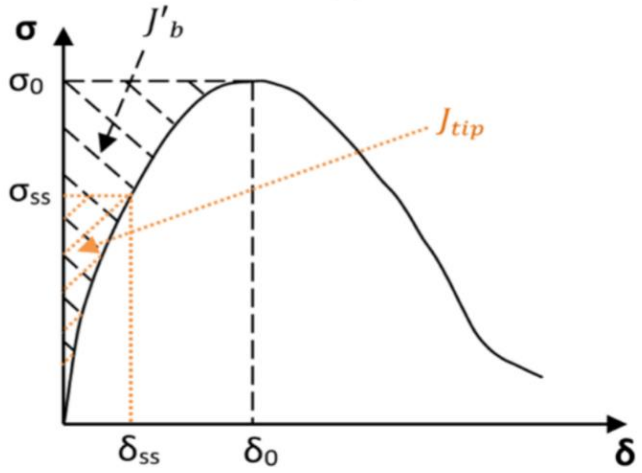


**Figure 2. Fiber bridging relation (stress-crack opening curve)(Arce et al., 2019).**

For a material to display PSH behavior, both the PSH strength index $(\sigma_0/\sigma_{fc})$ and the PSH energy index $(J_b'/J_{tip})$ must be greater than one. Fiber Reinforced Concrete's (FRC) tensile softening tendency takes place if either index drops below 1. The evidence from experiments has shown that $\sigma_0/\sigma_{fc} \geq 1.3$ and $J_b'/J_{tip} \geq 2.7$ are required to achieve robust tensile strain-hardening (Li, n.d.; Game et al., 2022).

While fiber and matrix/fiber interface characteristics, which define the stress-displacement relationship, have a sensitive impact on complementary energy of the fiber-bridging relation and

maximum fiber-bridging capacity, matrix parameters are seen to have an influence on crack tip matrix toughness and first-cracking strength. To connect the macro-scale composite PSH behavior to the micro-scale fiber/matrix interface characteristics, synergy among the fibers and the matrix is essential. These qualities can be used to replace regular concrete for ECC to enhance the structure's (Li, n.d.; Kanda et al., 2006). These properties are useful to replace the normal concrete for ECC to improve the structure's characteristics.

This innovative material not only improves concrete's resistance to cracking but also enhances its durability, making it an ideal solution for long-lasting and resilient infrastructure (Shumuye et al., 2023). When combined with materials like BCSA cement, these innovations create a powerful synergy that enhances both the durability and responsibility of concrete structures. This integration not only addresses the challenges of cracking and brittleness but also opens the door to longer-lasting, more resilient infrastructure solutions, especially in applications like pavements where tensile loading is a critical concern. The design of ECC aims at overcoming the essential shortcomings of conventional concrete, that is, the lack of tensile deformation capacity. As a result, ECC has a stress-strain curve that is more akin to that of a metallic material, having a distinctive "yield" strength followed by tensile strain-hardening behavior (Li, 2019).

## Corrosion

In PC concrete, the pH of the water found in the pores of the hardened concrete, also referred to as the pore solution, ranges from 12.5-13.5 (Mehta et al., 2006). This high pH condition leads to a passive protective film of hydroxides which form around the embedded steel and serves as protection from an anodic reaction (Mehta et al., 2006; Coppola et al., 2022). Since pH values between 12.5-13.5 are reached during mixing, passivation of embedded steel occurs rapidly after placement (Coppola et al., 2022).

The presence of chloride ions increases the risk of corrosion of reinforcing steel in concrete structures. In the absence of chloride ions in the pore solution, the passivity of steel is maintained at a pH above 11.5. In the presence of chloride ions in the pore solution, the passivity of steel can be compromised at a pH above 11.5, but the threshold value is variable based factors such as carbonation of concrete and relative humidity (Mehta et al., 2006; Coppola et al., 2022). The critical threshold of chloride ion concentration, or the threshold at which localized corrosion of embedded steel can initiate, is between 0.4-1% of cement weight (Coppola et al., 2022).

Concrete made with CSA cement has an initially lower pH than PC concrete, suggesting that they may have a lower resistance to corrosion of embedded rebar. A small amount of calcium hydroxide may be formed during hydration, depending on the relative quantity of calcium sulfate in the cement (Alapati et al., 2022). Any calcium hydroxide produced, in addition to oxides that remain inert during the hydration reaction, contribute to the alkalinity of the pore solution in BCSA cement concrete (Alapati et al., 2022). The resulting pore solution pH is lower than that of PC concrete (Mehta et al., 2006). Generally, the pore solution pH of PC concrete is 12-14 (Carsana et al., 2018a; Coppola et al., 2022), while BCSA cement concrete is around 11-12. This leaves the corrosion resistance of BCSA cement concrete as an open research question.

Previous research on PC concrete has shown several ways to protect reinforcing steel in concrete from corrosion. These may be subdivided into concrete surface treatments, mineral admixture inclusion, and chemical admixture inclusion.

Surface treatments with hydrophobic materials, such as silane, create a seal on any exposed air voids to prevent water and ion ingress (Coppola et al., 2022). Mineral admixtures can increase corrosion resistance in three ways: increasing time to corrosion initiation, passivation of steel reinforcement after corrosion initiation, and slowing the rate of corrosion (O'Reilly et al., 2019).

Partial replacements using Class C fly ash, Grade 100 slag cement, and silica fume were found to slow the rate to corrosion initiation (O'Reilly et al., 2019). These mineral admixtures create a denser microstructure, decreasing the overall permeability and therefore increasing carbonation and corrosion resistance, but the pozzolanic reactions they rely on may not operate the same way for a non-Portland cement.

Limited research is available on the effect of SCMs on the corrosion rate of embedded steel in CSA cement concrete. Chemical admixtures, such as nitrite-based chemicals, have also been shown as effective corrosion inhibitors (Coppola et al., 2022). Little research exists on the corrosion mechanics of embedded steel in concrete made with Alternative Cements (ACs), including CSA cements. Passivation of the embedded steel may occur slower than in PCC given its lower alkalinity to occur more rapidly than PCC. When carbonation of concrete occurs, pH drops, creating a condition that is conducive to embedded steel corrosion (Carsana et al., 2018b).

# Chapter 3. Materials and Methodologies

## 3.1 Materials

The materials used in the ECC portion of this study included coarse river sand, Type I PC, BCSA cement, OA, a high-range water reducer (HRWR), and polyethylene fibers. The materials used in the concrete portion of this study include crushed limestone coarse aggregate, coarse river sand fine aggregate, Type I/II PC, BCSA cement, class C fly ash (FA), HRWR, citric acid solution (CA), mild steel rebar and silane. All materials are described in detail in this section.

### 3.1.1 Crushed limestone

Locally available #57 gradation crushed limestone was used sourced from Hindsville, AR. It had a specific gravity of 2.66 and absorption of 0.48%.

## 3.1.2 Sand

For the ECC mixtures, coarse river sand with a maximum particle size of 0.5 mm was utilized, sieved through a #35 mesh sieve. Its specific gravity was measured as 2.62. For the concrete, study, coarse sand from the Arkansas River was used. It had a specific gravity of 2.61, fineness modulus of 2.87, and absorption of 0.523%.

### 3.1.3 Cementitious Materials

For ECC,

- Type I/II PC: Provided by Holcim, with a specific gravity of 3.15.
- BCSA Cement: Provided by CTS Cement, with a specific gravity of 2.98.
- Pozzolanic Material: OA, facilitated by Eco Materials, consists of a blend of ground bottom ash and fly ash. This material complies with ASTM C618-23 Class F requirements and has a specific gravity of 2.38.

For concrete,

- Type I/II PC: Ash Grove cement with specific gravity of 3.15.
- BCSA cement: Provided by CTS Cement with specific gravity of 2.96.
- FA: Class C FA provided by Eco Materials. Class C fly ash will be used as a mineral admixture to examine if passivation of reinforcing steel found in PCC occurs in BCSA cement concrete.

### 3.1.4 Admixtures

For both ECC and concrete,

- A polycarboxylate high-range water reducer (HRWR) was used to improve workability.
- Citric acid was added as a retarder to ensure adequate working time for mixing and molding due to BCSA cement's rapid-hardening properties.

### 3.1.4 Fibers

Ultra-high molecular weight polyethylene (PE) fibers were incorporated throughout the study. These fibers, with a density of 0.97 g/cm³, exhibit a tensile strength of 3900 MPa and an elastic

modulus of 145 GPa. Measuring 15 mm in length and 12 micrometers in diameter, they provide a length-to-diameter ratio of 800.

### 3.1.4 Mild steel rebar

Six meter (20 ft) lengths of grade 60 No. 13 (#4) deformed rebar were obtained for this research.

### 3.1.7 Silane

Silane is a frequently used hydrophobic surface treatment which protects concrete from aggressive exposure, such as saltwater (Coppola et al., 2022). A commercially available silane solution was obtained. The recommended application rate for this silane solution was 6.14-9.82 $m^2$/L (250-400 $ft^2$/gal) per coat. The manufacturer recommended two coats for porous surfaces such as concrete.

### 3.1.8 Characterization of Raw Materials

Illustrates the particle size distributions of ECC sand and cementitious materials. OA has a broader particle size distribution, indicating a mix of coarse and fine particles. Its distribution is more centered, with fewer particles in extremely fine or coarse ranges. PC and BCSA have smaller particle sizes compared to OA and Sand, essential for enhancing reactivity in cementitious applications. Sand has the largest particles, as expected, with a very steep increase in distribution around larger particle sizes.

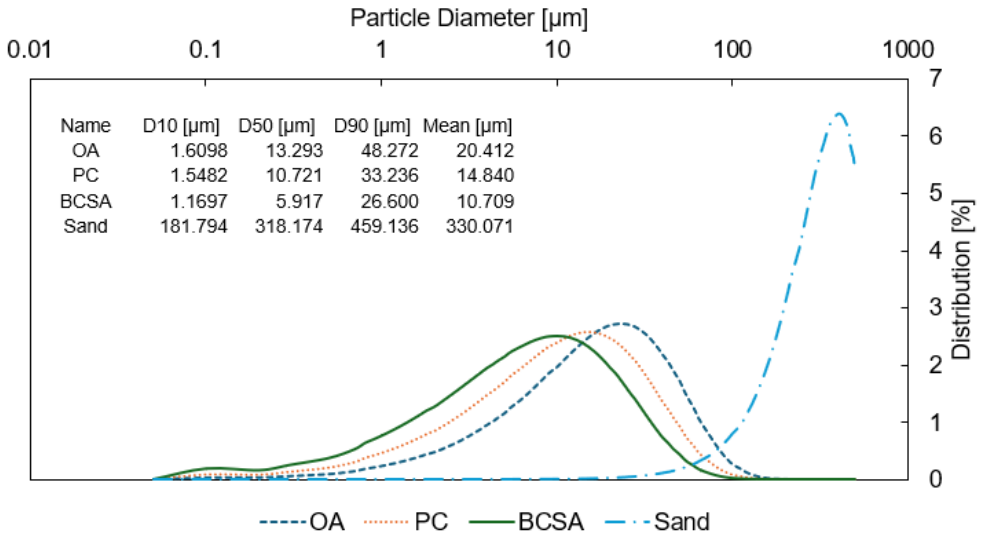


**Figure 3. Particle Size Analysis**

The chemical compositions and physical properties of PC, BCSA, and OA were analyzed using X-ray diffraction (XRD) and X-ray fluorescence (XRF) techniques as detailed in Table 1. OA complies with class-F coal ash chemical requirements per ASTM C618-23, having a moisture

content (MC) less than 3%, a loss on ignition (LOI) under 6%, $SO_3$ below 5%, and a combined content of $Fe_2O_3$ + $Al_2O_3$+ $SiO_2$ exceeding 75%.

**Table 1. Chemical Composition and Physical Properties of the Cementitious Materials.**

| (%) | PC | BCSA | OA |
|---|---|---|---|
| $Na_2O$ | 0.04 | - | 0.26 |
| MgO | 2.06 | 1.28 | 3.66 |
| $Al_2O_3$ | 6.26 | 19.46 | 19.43 |
| $SiO_2$ | 26.23 | 15.40 | 61.52 |
| $SO_3$ | 7.20 | 25.01 | 1.24 |
| $K_2O$ | 0.36 | 0.45 | 0.79 |
| CaO | 55.03 | 37.32 | 8.98 |
| $Fe_2O_3$ | 2.52 | 0.62 | 3.23 |
| Other | 0.31 | 0.46 | 0.89 |
| Quartz | - | - | 26.10 |
| Mullite | - | - | 13.90 |
| Labradorite | - | - | 60.00 |
| Ye'elimite | - | 27.20 | - |
| Anhydrite | - | 17.70 | - |
| Belite | 37.60 | 55.10 | - |
| Alite | 53.10 | - | - |
| Aluminate | 9.30 | - | - |
| LOI | 1.50 | 0.40 | 0.20 |
| MC | 0.50 | 1.40 | 0.40 |

Morphological characteristics were examined using scanning electron microscopy (SEM), with the images displayed in Figure 4. The PC's SEM image shows irregularly shaped particles with sharp edges. Particle morphology suggests a high surface area, which is beneficial for reactivity in cement hydration. BCSA cement's SEM image shows that the particles appear finer compared to PC, with smaller sizes visible in the SEM image. Sharp-edged particles are present, but the material appears more fragmented and uniform in size. This finer texture is consistent with the rapid hardening properties of BCSA cement, as smaller particles increase surface area and enhance reactivity. The OA image shows a mix of spherical particles (highlighted by arrows) and irregularly shaped particles. The spherical particles are typical of fly ash. The combination of spheres and irregular particles indicates a mix of fly ash and ground bottom ash. These features suggest pozzolanic reactivity, which contributes to strength development in cementitious systems. The sand image shows large, angular particles with rough surfaces. These particles are significantly larger than those of PC, BCSA, or OA, which aligns with sand's role as a structural aggregate in concrete.

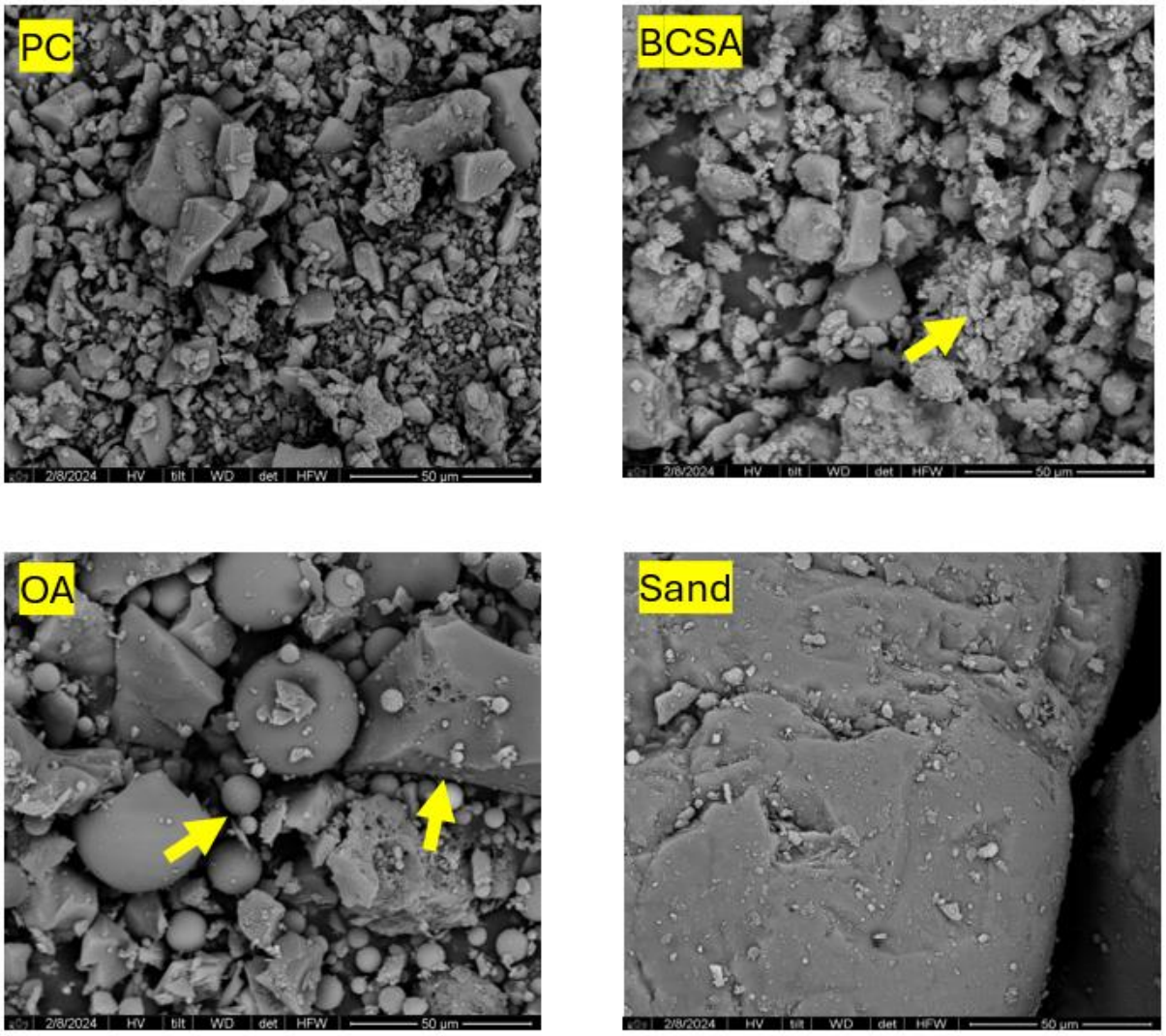


**Figure 4. SEM Images of PC, BCSA Cement, OA, and sand.**

## 3.2 Mixture Approach, Design and Procedure

### 3.2.1 ECC

BCSA cement was used to partially or completely replace PC to assess its effects on ECC properties. To investigate the influence of OA on ECC, two replacement levels for cement—55% and 70%—were utilized.

The mixture design parameters were consistent across samples: a water-to-binder (W/B) ratio of 0.27 and a sand-to-binder ratio of 0.36. The high-range water reducer (HRWR) was applied at a dosage of 7 ml per kilogram of cement to enhance workability.

Due to the rapid hardening nature of BCSA cement, which can be set within 10 minutes, the use of a retarder is critical to allow sufficient mixing time for ECC containing BCSA. For this purpose, a citric acid solution was prepared by dissolving 600 g of solid citric acid in 1 kg of water. This

solution was added at a rate of 8.8 ml per kilogram of BCSA cement, resulting in a citric acid concentration of 3.7 g per kilogram of BCSA (0.37% by weight).

The material proportions of the ECC mixtures used in the study are summarized in Table 2. The naming convention for each mixture follows the format Xm-YOA, where:

- X indicates the percentage of cement used,
- m refers to the type of cement (e.g., PC or BCSA), and
- Y represents the percentage of OA used as a replacement for cement.

For example, samples containing 50% PC and 50% BCSA cement with 55% OA are labeled as 50PC/50BCSA-55OA. This systematic design approach ensures clarity in understanding the mixed compositions and their respective roles in the study.

**Table 2. Material Proportions of the ECC Mixtures per 1 $m^3$**

| Specimen | OPC (Kg) | BCSA (Kg) | OA (Kg) | Sand (Kg) | Water (Kg) | Fibers (Kg) | HRWR (L) | CA (L) |
|---|---|---|---|---|---|---|---|---|
| 100PC-55OA | 589.2 | 0.0 | 707.0 | 466.6 | 350.0 | 11.8 | 4.1 | 0.0 |
| 50PC/50BCSA-55OA | 293.0 | 293.0 | 703.3 | 464.2 | 348.1 | 11.8 | 4.1 | 2.6 |
| 100BCSA-55OA | 0.0 | 583.0 | 699.6 | 461.8 | 346.3 | 11.8 | 4.1 | 5.2 |
| 100PC-70OA | 387.2 | 0.0 | 890.6 | 460.0 | 345.0 | 11.8 | 2.7 | 0.0 |
| 50PC/50BCSA-70OA | 193.0 | 193.0 | 887.6 | 458.5 | 343.8 | 11.8 | 2.7 | 1.7 |
| 100BCSA-2.3 OA | 0.0 | 384.6 | 884.5 | 456.9 | 342.7 | 11.8 | 2.7 | 3.4 |

*Note: PC=Portland cement, BCSA= belite calcium sulfoaluminate, OA = coal ash, HRWR= high range water reducer, and CA= citric acid solution*

All ECC mixtures were prepared using a planetary mixer following a systematic procedure. Initially, all powder materials (cements, sand, and OA) were dry-mixed for 30 seconds to ensure uniform distribution. For ECC mixtures containing BCSA cement, the CA was first combined with the mixing water and added to the mixer. Then, the mixing speed was then increased to 60 RPM, and the mix was blended for 60 seconds. The HRWR was subsequently introduced and mixing continued at the same speed for another 60 seconds, as per the supplier's instructions. Pre-dispersed PE fibers were added next, with mixing carried out at 60 RPM for 3 minutes to ensure uniform fiber distribution. The speed was further increased to 110 RPM for an additional 3 minutes to achieve a homogeneous mix. Once prepared, the ECC mix was cast into molds and subjected to 30 seconds of vibration to remove air bubbles and ensure proper compaction. After 24 hours at ambient temperature, the specimens were demolded and cured under specific conditions depending on their composition.

Mixtures without BCSA cement were cured in lime water at 23 ± 3°C, in accordance with ASTM C511, while mixtures containing BCSA cement (including partial content) were cured at 95% relative humidity (RH), as shown in Figure 5, and 23 ± 3°C, as per methods cited in the literature (Acarturk et al., 2023). These curing conditions were carefully chosen to prevent CH leaching from PC-only specimens, as lime water curing has been shown to negatively impact the compressive strength of BCSA-OA-based materials (Acarturk et al., 2023).

**Figure 5. BCSA based-ECC in the curing room**

### 3.2.3 Concrete

Concrete made with BCSA cement was evaluated in terms of compressive strength, ultrasonic pulse velocity (UPV) and corrosion resistance. Two w/cm, 0.36 and 0.44, were selected to represent a range large enough to yield significant differences in evaluated properties. In addition to w/cm, corrosion specimens were cast with varying cover depths of reinforcement, subjected to different moist curing times, some included 15% Class C fly ash (FA) replacement by cement weight, and some used silane surface treatment.

Mixture proportions are summarized in Table 3. All mixtures contained the same volume of coarse aggregate, 1068 kg/m$^3$ (1800 lb/yd$^3$). Class C FA replaced cement at a rate of 15% by mass for FA mixtures. FA mixtures therefore had different w/c, but identical w/cm to mixtures not containing FA.

A citric acid solution was prepared by dissolving 2265 grams (5 lb) of food grad citric acid in 3.8 liters (1 gallon) of potable water. This solution was added to each BCSA mixture at a dosage of 2.9 mL/kg (5 fl. oz/cwt) which yields a working time of approximately 45 minutes. This dosage of citric acid solution corresponds to 0.15% citric acid by weight of cement.

A commercially available polycarboxylate HRWR was used to increase workability without increasing water content. Dosages of HRWR were determined during trial batching to result in slump values of 175-225 mm (7-9 in.).

The naming convention used in Table 3 is in the form of cement type-FA (if applicable)-w/cm-mix number (if applicable). For example, BCSA 0.36-1 is a mixture using BCSA cement with w/cm=0.36 and was the first replicate mixture.

**Table 3: Concrete mixture proportions**

| Mixture | Cement, kg/m$^3$ (lb/yd$^3$) | Coarse agg., kg/m$^3$ (lb/yd$^3$) | Fine agg., kg/m$^3$ (lb/yd$^3$) | Water, kg/m$^3$ (lb/yd$^3$) | FA, kg/m$^3$ (lb/yd$^3$) | CA, mL/kg (fl. oz/cwt) | HRWR mL/kg (fl. oz/cwt) |
|---|---|---|---|---|---|---|---|
| BCSA 0.36 -1&-2 | 511 (861) | 1068 (1800) | 552 (930) | 184 (310) | - | 3.3 (5) | 3.9 (6) |
| BCSA 0.44 -1&-2 | 405 (682) | 1068 (1800) | 661 (1115) | 178 (300) | - | 3.3 (5) | 2.6 (4) |
| BCSA FA 0.36 | 434 (732) | 1068 (1800) | 552 (930) | 184 (310) | 77 (129) | 3.3 (5) | 3.9 (6) |
| BCSA FA 0.44 | 344 (580) | 1068 (1800) | 661 (1115) | 178 (300) | 60 (102) | 3.3 (5) | 2.6 (4) |
| PC 0.36 | 494 (833) | 1068 (1800) | 607 (1023) | 178 (300) | - | - | 2 (3) |
| PC 0.44 | 391 (659) | 1068 (1800) | 708 (1193) | 172 (290) | - | - | 0.7 (1) |

Concrete mixtures were mixed in two types of mixers: a 550 L (20 ft$^3$) capacity triple paddle drum mixer and a 150 L (5 ft$^3$) capacity rotary drum mixer. The steel paddles of the triple drum mixer revolve around an axle in the center of the drum. Rubber pieces are affixed to the steel paddles which extend to the inner surface of the drum, which scrape material from the inner walls of the drum as the paddles rotate. The rotary drum mixer has steel fins which add mixing energy to the mixture. The rotary drum mixer may be tilted to ensure proper mixing.

BCSA 0.36-1, 0.36-2, 0.44-1, 0.44-2, and PC 0.36, 0.44 were mixed using the triple paddle drum mixer due to the desired mix size and mixer capacity. Mixing in the triple paddle drum mixer requires a different order of material addition than as specified in ASTM C192: Standard Practice for Making and Curing Test Specimens in the Laboratory (ASTM Standard C192/C192M-19, 2019). Since BCSA cement is rapid hardening, shorter mixing times were preferred.

For BCSA mixtures in the triple paddle drum mixer, admixtures were incorporated into mixing water. CA was added to water which would be incorporated into the mixer first, and HRWR was added to water which would be incorporated into the mixer last. Mixing water containing CA was added to the mixer, the mixer was turned on and paddle rotation was turned on. Cement was added to the mixer followed by the remaining mixing water. Fine aggregate followed by coarse aggregate were added to the mixer. Approximately two minutes elapsed from the addition of BCSA into the mixer to the addition of coarse aggregate. Concrete mixed for four minutes from the addition of BCSA into the mixer. After four minutes, paddle rotation was paused and the mixer was powered down for a two minute rest period. After two minutes, the mixer was powered on again and paddle rotation occurred for an additional one minute. Concrete was then discharged from the mixer into wagons and transported to the area where fresh property testing and specimen casting occurred.

For PC mixtures in the triple paddle drum mixer, HRWR was incorporated into mixing water. The mixing procedure was identical to that of BCSA mixtures except concrete was mixed for five minutes from the addition of PC to the mixer, rested for three minutes, and mixed again for two minutes.

BCSA FA 0.36 and BCSA FA 0.44 were mixed in a rotary drum mixer due to the smaller mixture size. The order of material addition followed the order specified in ASTM C192 (ASTM Standard C192/C192M-19, 2019). A shorter mixing time was also preferred for BCSA FA mixtures due to the rapid hardening nature of BCSA cement.

Like BCSA mixtures in the triple paddle drum mixer, CA was added to mixing water which would be incorporated first and HRWR was added to mixing water which would be incorporated last. Coarse aggregate was added to the mixer followed by mixing water containing CA. The mixer was powered on and rotation began. Fine aggregate was added to the mixer and allowed to fully incorporate with coarse aggregate and water. BCSA and FA were added to the mixer and the remaining mixing water was added. Mixing time commenced with the addition of cement and FA to the mixer. Mixing occurred for three minutes, rested for two minutes, and mixed again for one minute Concrete was then discharged from the mixer into wagons and transported to the area where fresh property testing and specimen casting occurred.

## 3.3 Test Methods

### 3.3.1 Flow Test

The workability of the fresh ECC mixtures was assessed using the flow table test, conducted in accordance with ASTM C1437-20(ASTM, 2020). The flow table and flow mold used adhered to the specifications outlined in ASTM C230(ASTM, 2021; 2023) as shown in Figure 6. This test provided a measure of the ease of handling and placing the fresh ECC mixtures.

**Figure 6. BCSA-ECC mixture after completion of flow test**

### 3.3.2 Slump

The workability of fresh concrete was measured according to ASTM C143: Standard Test Method for Slump of Hydraulic-Cement Concrete (ASTM Standard C143/C143M-20, 2020). The dosage of HRWR was adjusted for each mixture during the trial batching phase to yield slump values of 175-225 mm (7-9 in.).

### 3.3.3 Density

The density of concrete was measured according to ASTM C138: Standard Test Method for Density, Yield, and Air Content of Concrete (ASTM Standard C138/C138M-24a, 2024).

### 3.3.4 Air content

The air content of concrete was measured according to ASTM C 231: Standard Test Method for Air Content of Freshly Mixed Concrete by the Pressure Method (ASTM Standard C231/C231M-24, 2024). A type B meter was used to measure air content.

### 3.3.5 Setting Time

The setting time of the fresh mortars was evaluated using the penetration test, following ASTM C191-21(ASTM, 2021) as shown in Figure 7. To avoid false readings, no fibers were included in the mixture during this test. The initial setting time was defined as the time required for the penetration needle to reach a depth of 25 mm, while the final setting time was recorded when the needle could no longer penetrate the mortar. All tests were conducted at an ambient temperature of 22 ± 2ºC.

**Figure 7. Setting time set up**

### 3.3.6 Compressive Tests and Bulk Density

The compressive strength of the ECC mixtures was evaluated using 50 mm x 50 mm x 50 mm (2 in. x 2 in. x 2 in.) cube specimens, prepared and tested according to ASTM C109M-21(ASTM, 2019). Three specimens were tested for each mixture at curing ages of 1 day, 7 days, and 28 days. Compression tests were performed using a hydraulic testing machine at a constant loading rate of 0.25 MPa/s as shown in Figure 8. Moreover, the bulk density of ECC mixtures was calculated with the weight and dimensions of the cube at 28 days.

**Figure 8. Compressive strength test**

Compressive strength of 10 cm x 20 cm (4 in. x 8 in.) cylinders was evaluated. These cylinders were cast according to ASTM C192 (ASTM Standard C192/C192M-19, 2019). Three replicates were cast for each testing age. For BCSA cement-based mixtures, testing occurred at four hours, six hours, one day, three days, seven days,14 days, 28 days, 56 days, and 90 days. For PC mixtures, testing occurred at one, three, seven,14, 28, 56, and 90 days.

After surface finishing, cylinders were covered with plastic to reduce moisture loss from evaporation and allowed to cure at ambient conditions for 24 hours. After 24 hours, cylinders were removed from their molds using compressed air and end ground with an automatic feed diamond coated blade to ensure ends were plane and perpendicular to the cylinder sides. Height and average diameter measurements were recorded for each cylinder before placement in a moist curing chamber held at a constant 100% RH and 23±2°C (73.5±3.5°F). Cylinders tested at four hours, six hours and one day were not moist cured. Approximately 24 hours prior to testing time, cylinders were removed from the 100% RH curing chamber and placed in a dry curing chamber held at 50% ±2% RH and 23±2°C (73.5±3.5°F).

Compressive strength of concrete mixtures was evaluated according to ASTM C39: Standard Test Method of Cylindrical Concrete Specimen (ASTM Standard C39/C39M-21, 2021). Cylinders were placed in a high stiffness load frame and centered visually on concentric circles on the self-leveling head, shown in Figure 9. A preload of approximately 10% of the anticipated ultimate load was placed on the cylinders before loading at a rate of 0.24 MPa/sec (35 psi/sec). Anticipated ultimate loads were estimated from the results of trial batching. Ultimate load (kN, lbf) was recorded and ultimate compressive stress, or compressive strength, $f_c$, was calculated based on the average diameter.

**Figure 9: Compressive strength test on cylinders**

### 3.3.7 Tensile Tests

To evaluate the tensile properties of the different ECCs, uniaxial tensile tests were conducted following the recommendations of the Japan Society of Civil Engineers (JSCE, 2008). Five dumbbell-shaped specimens, with an effective testing area of 13 mm x 30 mm x 80 mm as shown in Figure 10, were prepared and tested after 1, 7, and 28 days of curing for each ECC mixture.

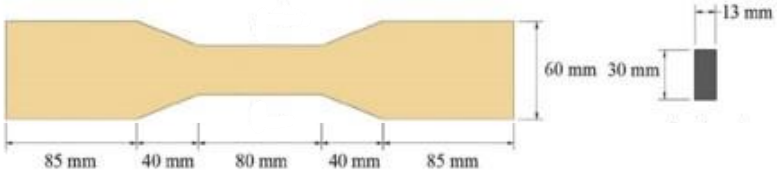


**Figure 10. Dogbone dimension for uniaxial tensile testing**

The tests were performed using a displacement control procedure at a loading rate of 0.5 mm/min. The tensile properties of the mixtures were further analyzed using dogbone-shaped specimens, with the geometric dimensions and test setup illustrated in Figure 10. For samples at 1-day and 7-day, a load cell of 5KN was used, and the tensile strain capacity within the gauge length was measured using digital image correlation, utilizing dots as reference points for the change in length, as shown in Figure 11. For samples on 28-day, a load cell of 250KN was used and the tensile strain capacity within the gauge length was measured with LVDTs, as shown in Figure 12.

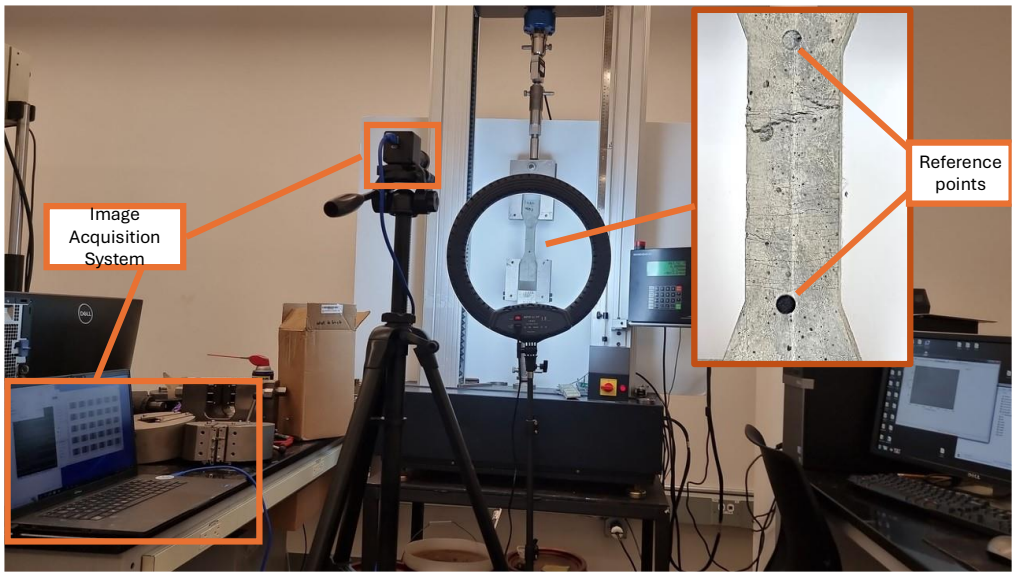


**Figure 11. Image acquisition system set up for the uniaxial tensile test at 1 and 7 days**


**Figure 12. Set up for the uniaxial tensile test for 28 days**

### 3.3.8 Crack Analysis

Following the uniaxial tensile tests at 28 days, the ECC specimens were analyzed in detail to evaluate their cracking behavior. A digital microscope was used to examine the crack size and microstructure, while digital image analysis provided additional insights into the mean and maximum crack widths. These measurements were critical for understanding the material's durability and impermeability.

Images of the cracks were captured and manually labeled using the open-source tool VIA Image Annotator. The annotation file was then imported into Python, where crack width measurements were performed. The average crack width for each crack was determined by sampling the width at 30 different locations along its length. The overall average crack width for a specimen was

calculated by averaging all individual crack width measurements. Additionally, the number of cracks per dogbone specimen was quantified to provide a comprehensive assessment of cracking behavior.

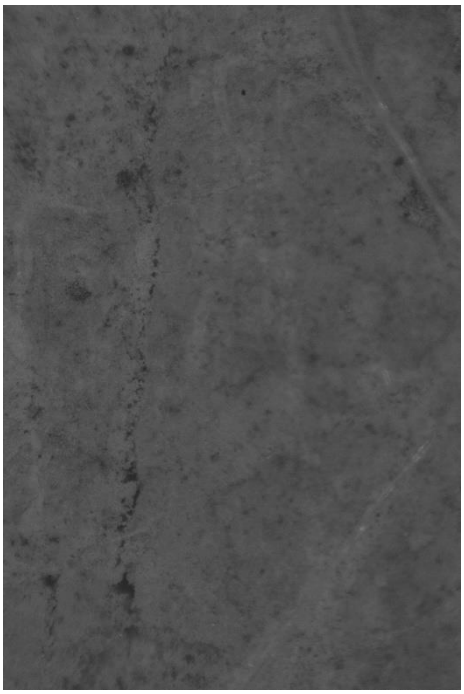

**Figure 13. Crack of a BCSA-ECC specimen seen through a digital microscope**

### 3.3.9 Flexural Test

A third-point bending test was conducted in accordance with ASTM C1609 (ASTM, 2024c) using a servo-hydraulic universal testing system to evaluate the flexural strength and deformation capacity of the ECC material. The three best mixture performing replicates prismatic specimens with dimensions of 101.6 mm × 101.6 mm × 355.6 mm (4 × 4 × 14 in) were cast and tested after 28 days of curing.

The testing followed a four-point loading setup determining key parameters such as first-peak strength, ultimate strength, and deflection. The load was applied at a rate of 0.075 mm/min, while the midspan net deflection and applied load were continuously recorded using an automated data acquisition system. To accurately measure deflection, two LVDTs were attached to the testing setup, as illustrated in Figure 14.

During testing, specimens were subjected to a controlled loading rate until failure, and their load-deflection responses were analyzed. The flexural strength (modulus of rupture) was calculated using the peak load and specimen geometry. Post-cracking behavior, including deflection-hardening and residual strength, was evaluated to assess the material's ability to sustain load-bearing capacity after cracking.

The energy absorption capacity (toughness) was also determined by integrating the area under the load-deflection curve, providing insights into the material's fracture resistance and ductility. Observations of crack patterns and fiber distribution were conducted to further understand the interaction between fibers and the cementitious matrix.

**Figure 14. Flexural strength test.**

### 3.3.10 Ultrasonic Pulse Velocity (UPV)

Ultrasonic pulse velocity (UPV) is a nondestructive test which can be used to estimate characteristics of hardened concrete such as dynamic modulus of elasticity, dynamic Poisson's ratio, and density. UPV of cylinders was evaluated immediately before compressive strength testing according to ASTM C597: Standard Test Method for Ultrasonic Pulse Velocity Through Concrete using the commercially available UPV measurement device shown in Figure 15 (ASTM Standard C597-22, 2022). Transducer targets were marked on the ends of each cylinders using permanent marker and ring-shaped stencil with 10 cm (4 in.) outer diameter and 5 cm (2 in.) inner diameter. A nickel sized dollop of commercially available water-soluble ultrasound gel was placed on the end of each UPV transducer and transducers were pressed firmly on the ends of each cylinder, taking care to align transducers with the drawn-on targets. Wave transit time was recorded and UPV was calculated using the measured height of the cylinder.


**Figure 15: UPV Measurement Device**

### 3.3.11 Corrosion Tests

Corrosion testing was performed according to ASTM G109: Standard Test Method for Determining Effects of Chemical Admixtures on Corrosion of Embedded Steel Reinforcement in Concrete Exposed to Chloride Environments (ASTM Standard G109-21, 2021). No. 13 (#4) grade 420 (60) rebar was obtained and cut into 381 mm (15 in.) pieces. Both ends were faced, and one end was drilled and tapped. Two 316 stainless steel nuts were placed on the end of 4.8 mm (0.19 in.) diameter, 25 mm (1 in.) long, 316 stainless steel screws with 10-24 thread size. The screws were fastened into the drilled and tapped ends, leaving both nuts and approximately 6.25 mm (0.25 in.) of the shank exposed.

Rebar pieces were sent to a local, commercial sandblaster to remove all surface rust and mill scale and was returned to near white metal. Rebar was soaked in hexane then stored in an airtight container with desiccant bags to prevent rust formation prior to preparation and testing.

An example of a prepared rebar sample is shown in Figure 16. Commercially available electroplaters tape was wrapped on the ends of the rebar, leaving approximately 203 mm (8 in.) exposed rebar in the middle. Copper wire was wrapped around the shank of the screw between the two nuts and the nuts were tightened together to hold the wire in place. Electrical continuity between the wire and the rebar was tested using a multimeter. 3 mm (0.125 in.) neoprene tubing was placed over the last 7.6 mm (3.5 in.) of the rebar and the screw, leaving the free end of the copper wire exposed. A commercially available two-part waterproof epoxy meeting the requirements of Type IV, Grade 3, Class E according to ASTM C881: Standard Specification for Epoxy-Resin-Base Bonding Systems for Concrete was placed in the ends of the neoprene tubing to create a waterproof seal (ASTM Standard C881/C881-20a, 2020).

**Figure 16: Prepared rebar specimen**

Formwork was fabricated from coated plywood to create 280 mm x 115 mm x 190 mm (LxWxH, 11 in. x 4.5 in. x 7.5 in.) rectangular prisms. The height dimension differs from the 150 mm (6 in.) height described in ASTM G109 because an integral dam for saltwater ponding with height of 38 mm (1.5 in.) was cast into the concrete rather than placing one on top of the finished specimen. The dimensions of the formwork blockout used to create the integral dam are shown in Figure 17. A trapezoidal shaped blockout was selected over a rectangular prism shaped blockout for ease of removal from concrete after casting. The exposed area of the concrete to saltwater (76 mm x 150 mm) was the same as the plexiglass dam described in ASTM G109. The 76 mm x 178 mm (4 in. x 7 in.) surface of the formwork blockout was attached to the bottom inside face of the rectangular prism formwork using wood screws.

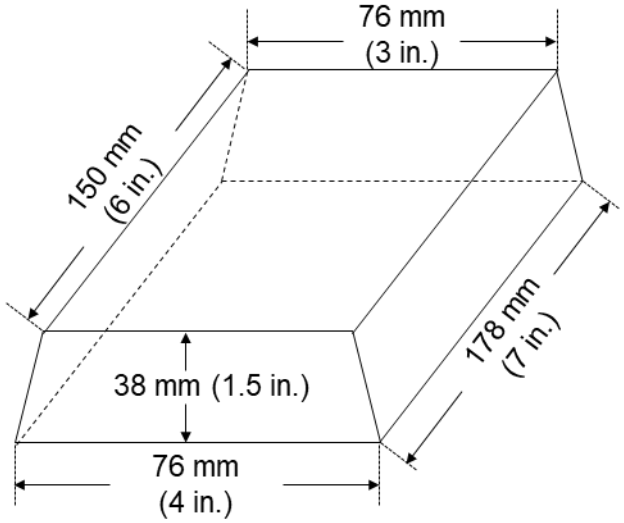


**Figure 17: Integral dam blockout**

A surface coating of form release oil was placed on the formwork and integral dam blockout immediately before prepared rebar pieces were placed through holes in formwork end pieces are shown in Figure 18. Since the formwork blockout creates an integral dam at the top of specimens, specimens were cast in an upside-down orientation. Therefore, one piece of prepared rebar was placed at 25 mm (1 in.), 38 mm (1.5 in), or 51 mm (2 in.) clear vertical distance from the formwork blockout and equidistant from each vertical face of the formwork. Two pieces of prepared rebar were placed with 25 mm (1 in.) clear vertical distance from the top (as cast) surface of the formwork and at least 25 mm (1 in.) clear horizontal distance from the vertical faces of the formwork.

**Figure 18: Prepared rebar pieces in formwork**

Concrete from the same batch as used for companion cylinders was cast into forms in two approximately equal lifts and consolidated with a stinger type internal vibrator. The tops of specimens were finished with a wooden float until flush with the top of the formwork, covered with plastic to avoid moisture loss through evaporation and allowed to cure at ambient conditions for 24 hours. After 24 hours, specimens were removed from formwork, labeled with permanent marker, and placed in the moist curing chamber described in the 3.3.6 Compressive Tests and Bulk Density section. The dimensions of specimens after removal from formwork are shown in Figure 19. The variable clear vertical distance between the integral dam and the top piece of rebar was selected to correspond to depths according to ASTM G109 (25 mm, 1 in.) and typical cover depths for structures according to 20.5.1.3.1: Specified concrete cover for cast-in-place nonprestressed concrete members (38 mm & 51 mm, 1.5 in. & 2 in., respectively) in ACI 318-19: Building Code Requirements for Structural Concrete and Commentary (ACI Committee 318, 2019).

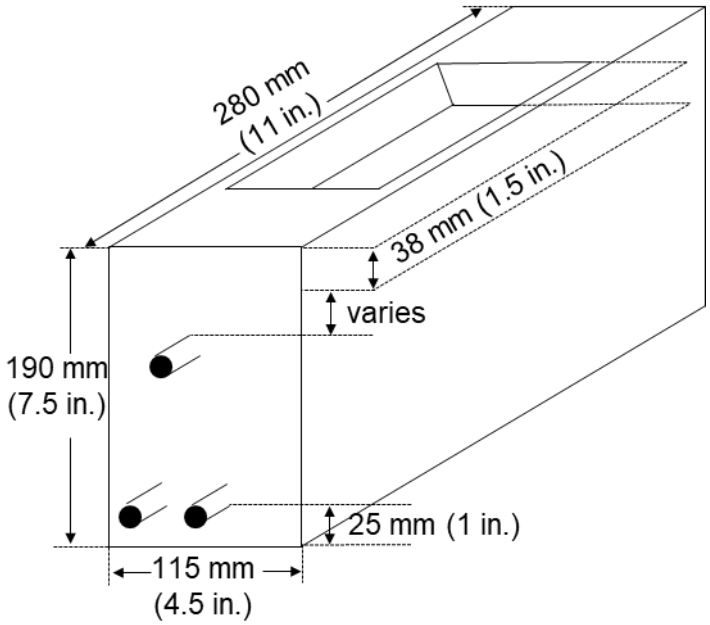


**Figure 19: Dimensions of finished corrosion specimens**

Several specimen sets were cast from each concrete mixture, summarized in Table 4 for w/cm=0.36. The same specimen sets were cast for w/cm=0.44. Each row in Table 4 represents a set of three replicates. Casting all specimens with the same w/cm was not possible due to limitations in mixer capacity. Therefore, for both w/cm, the first mixture cast included specimen sets with 25 mm (1 in.) cover depth and moist curing time of 28 and 90 days. For both w/cm, the second mixture cast included specimen sets with 25 mm (1 in.), 38 mm (1.5 in.), and 51 mm (2 in.) cover depths and moist curing times of 7, 28, and 90 days. Specimens cast with 15% FA replacement and specimens cast with PC were cast from one batch, respectively.

**Table 4: Corrosion specimen matrix for w/c=0.36**

| Concrete Mixture Name | Cover Depth, mm (in.) | Moist Cure Time, days | Additional Variation |
|---|---|---|---|
| BCSA 0.36-1 | 25 (1) | 28 | - |
| BCSA 0.36-1 | 25 (1) | 90 | - |
| BCSA 0.36-1 | 25 (1) | 90 | Silane surface treatment |
| BCSA 0.36-2 | 25 (1) | 7 | - |
| BCSA 0.36-2 | 38 (1.5) | 28 | - |
| BCSA 0.36-2 | 51 (2) | 28 | - |
| BCSA 0.36-2 | 38 (1.5) | 90 | - |
| BCSA 0.36-2 | 51 (2) | 90 | - |
| BCSA 0.36 FA | 25 (1) | 90 | 15% FA replacement |
| PC 0.36 | 25 (1) | 28 | - |

After moist curing for the selected time was complete, specimens were removed and surface dried before wire brushing the finished surfaces. Dust was removed using compressed air and the

samples were placed in the dry curing chamber described in 3.3.6 Compressive Tests and Bulk Density for two weeks. After two weeks, specimens were removed from the dry curing chamber and a commercially available epoxy sealer meeting the requirements for Type III, Grade 1, Class C according to ASTM C881 applied to the vertical sides and top surface of specimens excluding the integral dam area (ASTM Standard G109-21, 2021; ASTM Standard C881/C881-20a, 2020). Two coats of silane surface treatment was applied to the specimens receiving a silane surface treatment at a rate of 6.14 $m^2$/L (250 $ft^2$/gal). Specimens were moved back to the dry curing chamber for 24 hours while the epoxy sealant cured. Specimens were then moved to the storage and testing area for the remainder of the study.

Specimens remained in the storage and testing area undisturbed for 14 days following the initial removal from the dry curing chamber. Then, the dam was filled with a 3% NaCl solution, by mass, and plastic was loosely placed on top of specimens to prevent evaporation. The solution remained in the integral dam for 14 days and was topped up when necessary. The 14 days of NaCl exposure is referred to as a ponding cycle. Seven days into the ponding cycle, macrocell measurements were taken using a multimeter. Voltage across the 10 Ω resistor was measured using a high impedance multimeter, shown in Figure 20. The common terminal was placed on the wires corresponding with bottom bars and the positive terminal was placed on the wire corresponding to the top bar. This configuration creates readings which correspond to an anodic top bar and cathodic bottom bars, or positive galvanic current.

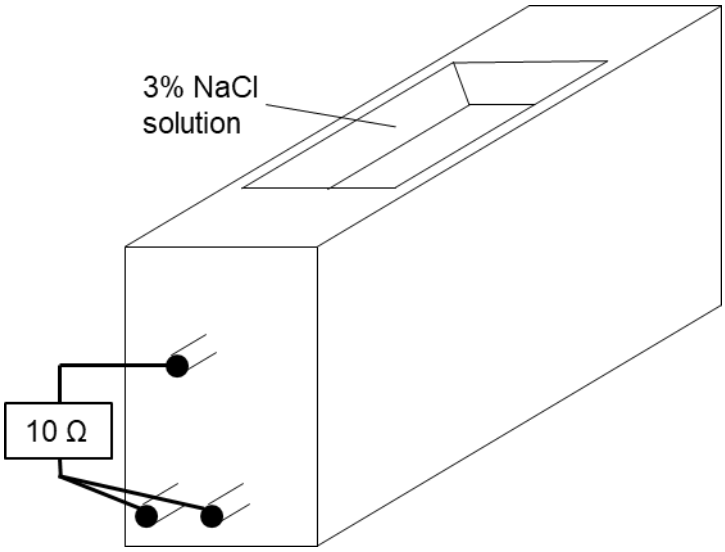


**Figure 20: Corrosion testing set up**

Macrocell current, I, was calculated using the voltage measured across the resistor according to Equation 4.

$$I_j = V_j / 10$$

**Equation 4**

where,

$I_j$ = macrocell current at time j (amps)

$V_j$ = measured voltage at time j (volts)

A total integrated current, or total corrosion (TC) value of 150 coulombs (C) for at least half the specimens indicates the end of the testing period or when the average total integrated current of control specimens exceeds 150 C.TC is calculated according to Equation 5.

$$TC_j = TC_{j-1} + [(t_j - t_{j-1}) \times (i_j + i_{j-1})/2]$$

**Equation 5**

where,

TC = total corrosion (coulombs)

$t_j$ = time at which measurements are taken (seconds)

$i_j$ = macrocell current at time $t_j$ (amps)

At the end of each ponding cycle, the NaCl solution was removed using a sponge and the specimen was undisturbed for 14 days. This 14-day undisturbed cycle is referred to as a drying cycle.

# Chapter 4. Results and Discussions

## 4.1 Flow Test

Figure 21 illustrates the results of the flow table test conducted on various ECC mixtures in their fresh state. A clear trend was observed: increasing the OA content from 55% to 70% as a cement replacement resulted in improved fluidity of the mixtures. This enhancement in workability is primarily attributed to the morphology of OA, which is characterized by predominantly spherical particles, with only minor impurities of irregular shapes.

The spread diameters of ECC mixtures containing 100% BCSA and 100% PC, at both OA replacement levels, were found to be comparable. Previous studies have reported spread diameters of PC-based ECC ranging from 160 to 180 mm and CSA-based ECC ranging from 140 to 210 mm (Game et al., 2022; Xie et al., 2023). The spread diameters observed in this study fall within these ranges, indicating consistency with existing research. These results confirm that the ECC mixtures developed in this study exhibit acceptable flow properties, as demonstrated by the flow table test.

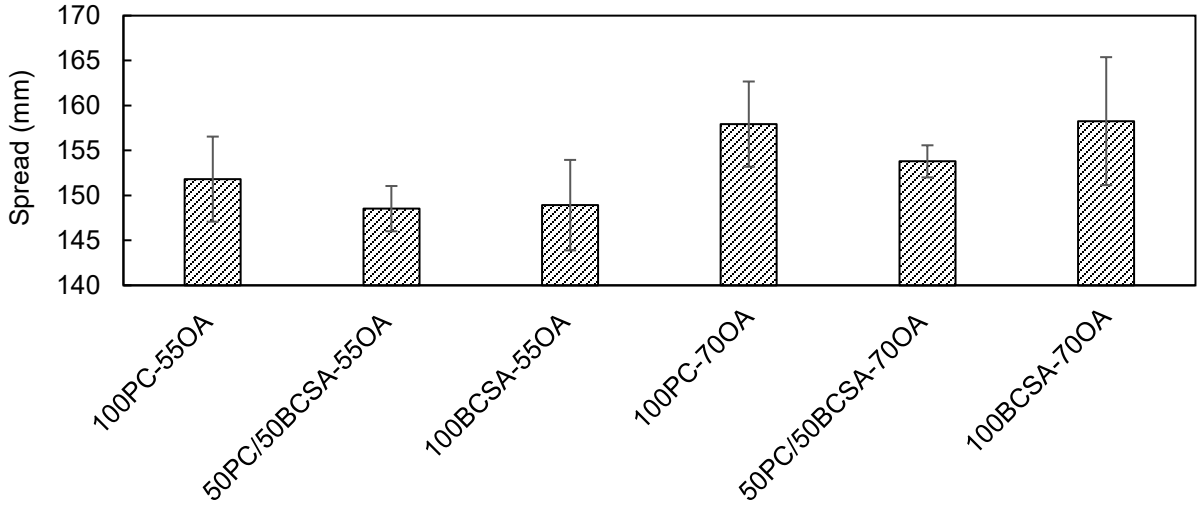


**Figure 21. Spread Diameter of PC-ECC, PC/BCSA-ECC, and BCSA-ECC**

## 4.2 Setting Time

Figure 22 presents the results of the setting time tests for samples containing BCSA cement at replacement levels of 50% and 100%. The initial setting time for samples made entirely of PC exceeded 180 minutes, and these were excluded from the analysis. The data in Figure 22 reveal two notable trends: (1) Increasing the BCSA cement content from 0% to 50% and then to 100% significantly reduced the setting time, and (2) The incorporation of PC into the mix led to an increase in setting time.

The reduction in setting time observed with higher BCSA content can be attributed to the early hydration of BCSA cement. During this process, anhydrite and ye'elimite (as shown in Table 1) react to form ettringite, the primary crystalline phase (Burris et al., 2022; Yoon et al., 2021). It is hypothesized that the presence of PC reduces the overall content of ettringite, causing a delay in the setting time.

These findings are consistent with prior research, which reported initial and final setting times of 13 and 32 minutes, respectively, for BCSA cement paste with a similar water-to-cement ratio and CA content (Burris et al., 2022). The results from this study corroborate those observations, confirming the influence of BCSA cement on setting time and reinforcing the observed trends.

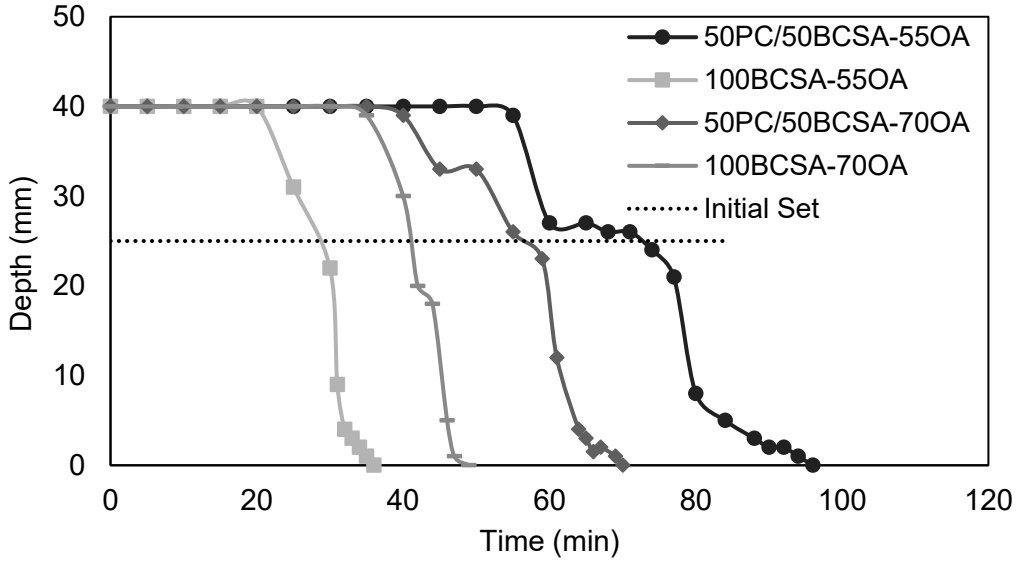


**Figure 22. Setting Time of PC/BCSA and BCSA mixtures**

## 4.3 Slump, Density and Air Content

Results from slump, density and air content tests on concrete mixtures used in the corrosion testing are summarized in Table 5. The inclusion of FA increased the slump of both w/cm mixtures. The spherical particle shape of FA acted as ball bearings, increasing slump. Also, since FA does not react with water and BCSA cement reacts rapidly with water, cement replacement with FA effectively increased with free water content, which also increased slump. The HRWR dosage could have been reduced with FA mixtures but was kept consistent with cement only mixtures.

Densities of mixtures were consistent within cement types. BCSA cement has a lower specific gravity than PC, so lower densities were expected from BCSA mixtures compared to PC mixtures. Air content for all mixtures was consistent. Since no air entraining admixtures were included, only entrapped air was expected.

**Table 5: Slump, Density and Air Content Results**

| Mixture | Slump, mm (in.) | Density, kg/m$^3$ (lb/ft$^3$) | Air Content, % |
|---|---|---|---|
| BCSA 0.36-1 | 229 (9) | 2345 (146.4) | 2.8 |
| BCSA 0.36-2 | 229 (9) | 2337 (145.9) | 3.0 |
| BCSA FA 0.36 | 254 (10) | 2321 (144.9) | 2.7 |
| PC 0.36 | 190.5 (7.5) | 2378 (148.4) | 2.3 |
| BCSA 0.44-1 | 248 (9.75) | 2318 (144.7) | 3.4 |
| BCSA 0.44-2 | 229 (9) | 2319 (144.8) | 2.7 |
| BCSA FA 0.44 | 248 (9.75) | 2357 (147.1) | 2.7 |
| PC 0.44 | 139.7 (5.5) | 2380 (148.6) | 2.2 |

## 4.4 Compressive Strength

Figure 23a and 23b present the compressive strength development of various ECC mixtures at 1, 7, and 28 days for both cement replacement levels with OA. The data highlight distinct trends in strength development at different curing stages. At 1 day of curing, the mixture with 100% BCSA cement and 55% cement replacement with OA (100BCSA-55OA) exceeded the minimum required compressive strength of 31 MPa required for conventional concrete (LaDOTD, 2016). By 7 days, the 100BCSA-55OA and 100PC-55OA mixtures also surpassed compressive strength threshold. By 28 days, all mixtures, except for 100BCSA-70OA, surpassed the 31 MPa benchmark.

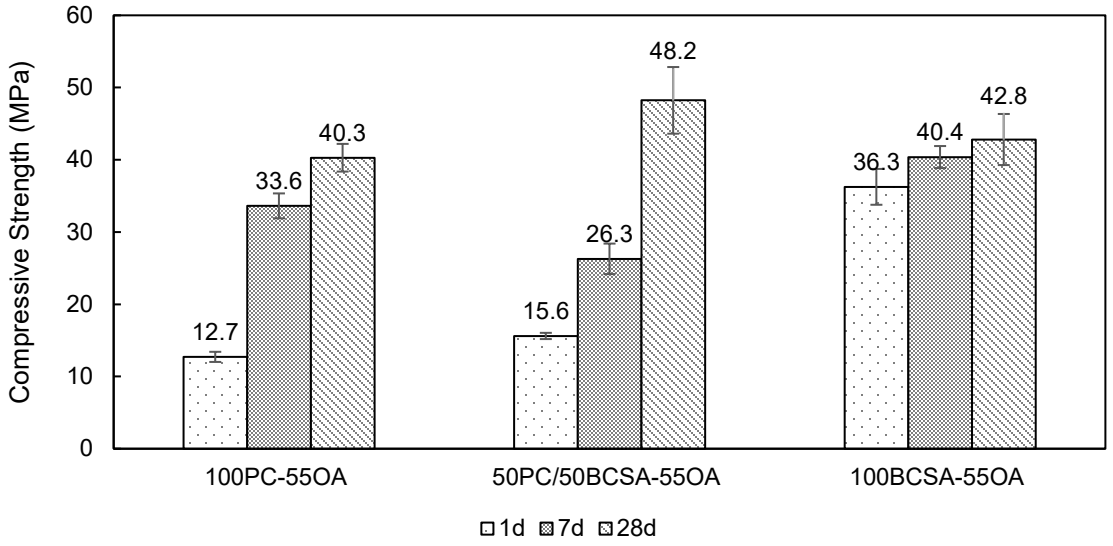


(a)

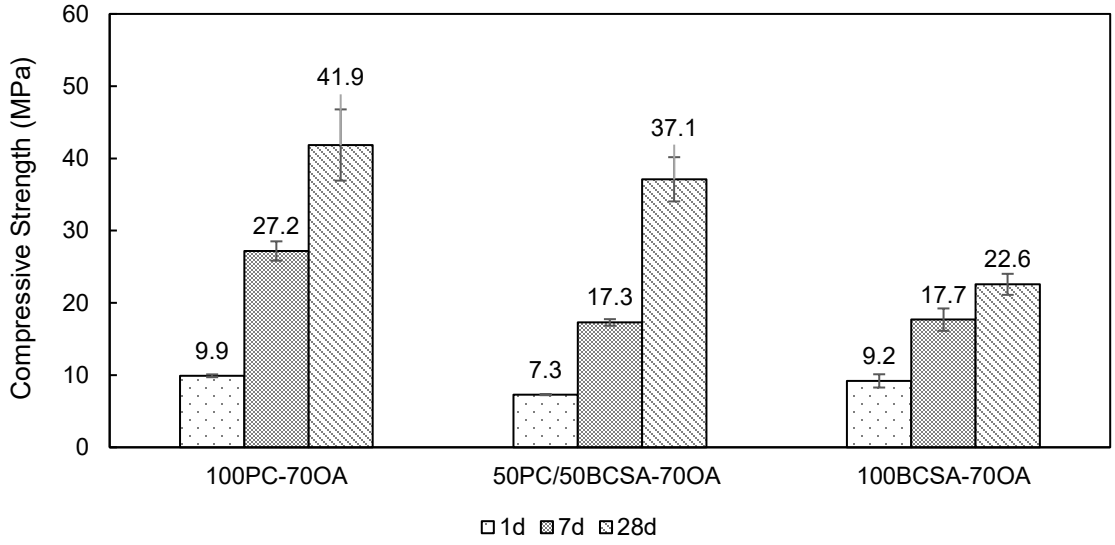


(b)

**Figure 23. Compressive Strength at 1, 7, and 28 days (a) ECCs with 1.2 OA ratio, and (b) ECCs with 2.3 OA ratio**

The development of strength is shown in Table 6. Mixtures with 100% PC perform well in terms of early (1-7 days) and overall (1-28 days) strength gains, especially at higher OA levels. This highlights PC's ability to sustain hydration reactions in the presence of OA (Şahmaran et al., 2015; Mindess, 2019). On the contrary, mixtures with 100% BCSA exhibit limited strength gains after the early stage, as hydration occurs rapidly within the first day, leaving little for later development. Mixtures with 50% PC and 50% BCSA achieve the highest strength gains, with significant strength development in the 7 to 28 days period, particularly at higher OA levels. This suggests that the

combination of PC and BCSA optimizes hydration kinetics and leverages the pozzolanic activity of OA (Şahmaran et al., 2015; Mindess, 2019).

**Table 6. Compressive strength gains over days.**

| Specimen | 1-7 days | 7-28 days | 1-28 days |
|---|---|---|---|
| 100PC-55OA | 164% | 20% | 217% |
| 50PC/50BCSA-55OA | 68% | 83% | 209% |
| 100BCSA-55OA | 11% | 6% | 18% |
| 100PC-70OA | 174% | 54% | 323% |
| 50PC/50BCSA-70OA | 137% | 115% | 408% |
| 100BCSA-70OA | 92% | 28% | 145% |

At 55% OA replacement, mixtures containing 100% BCSA exhibited the highest early compressive strength due to the rapid hydration and ettringite formation characteristic of BCSA cement (Cai et al., 2023; Acarturk et al., 2023). However, by 28 days, the 50PC/50BCSA-55OA mixture achieved the highest compressive strength (48.2 MPa), highlighting the synergistic effect of combining PC and BCSA for sustained strength development.

In contrast, mixtures with 70% OA replacement showed reduced early and long-term strength across all compositions. At this level, 100% PC mixtures demonstrated the highest 28-day compressive strength (41.9 MPa), indicating that PC is better suited for higher OA replacement levels due to its ability to accommodate the slower pozzolanic reaction of OA. This suggests delayed hydration processes facilitated by the reaction of CH and the amorphous content of OA, which continues as long as CH is present (Şahmaran et al., 2015; Mindess, 2019). The reduction in compressive strength observed with increasing OA content in the 50PC/50BCSA and 100BCSA mixtures can be attributed to several key factors. In mixtures containing PC, a high OA-to-cement (OA/C) ratio can inhibit secondary hydration reactions that are critical for strength development. In such cases, OA primarily acts as a pore-filling material. Due to the pore-filling effect of the fly ash, the gel space ratio of the concrete increases, which could improve the matrix's overall strength and fracture toughness (Kameswara Rao et al., 2022). In mixtures with 100% BCSA, OA functions as a diluter, reducing the concentrations of anhydrite and belite, which are essential for developing the matrix's structural integrity, as highlighted by García-Maté et al. (García-Maté et al., 2013). Furthermore, the pozzolanic reaction of OA is relatively slow at early days, with its effects becoming more pronounced after 28 days and particularly beyond 90 days, indicating that its contribution to strength development remains incomplete within the initial 28-day period (Cheriaf et al., 1999).

Hence, two clear trends can be described after this analysis: (1) BCSA excelled in early strength development, (2) while PC mixtures exhibited greater relative strength gains over time, especially at higher OA replacement levels. These findings underscore the importance of optimizing the balance between PC, BCSA, and OA content to achieve desired strength performance at both early and long-term curing stages.

The compressive strength gain of concrete cylinders from the corrosion study with w/cm=0.36 as a function of time is shown in Figure 24. Samples made with BCSA 0.36-1 and BCSA 0.36-2 mixtures have the highest compressive strength throughout the evaluation period. A drop in compressive strength at 56-days for BCSA 0.36-1 indicates a possible error in testing, poor consolidation, or other anomaly. BCSA 0.36-1 and BCSA 0.36-2 were cast using different

production runs of BCSA cement. The greatest difference in compressive strength between BCSA 0.36-1 and 0.36-2 occurs at extreme early ages, i.e. four and six hours, which have differences of 9.5% and 8.1%, respectively. At later age, such as 90 days, the difference in compressive strength was 1.9%. It appears that at extreme early ages, some difference in cement reactivity due to age and production runs contributed to differences in compressive strength. At other ages, the low w/cm paired with the high cement content, 511 kg/m$^3$ (861 lb/yd$^3$) negated any potential difference in cement reactivity due to age and production runs.

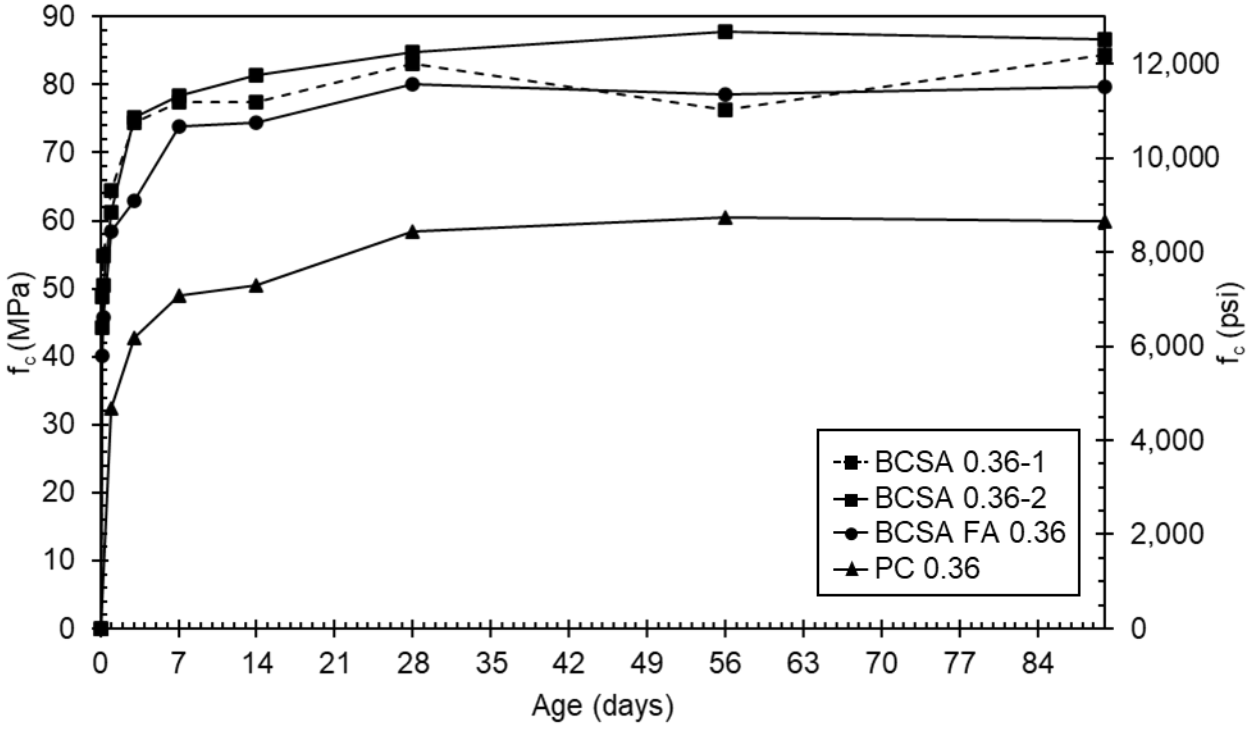


**Figure 24: Compressive strength gain for w/cm=0.36 mixtures**

BCSA 0.44 FA was cast using the same production run of BCSA 0.36-2. BCSA FA 0.36 shows the effect of a 15% replacement of FA, thought to be inert when mixed with BCSA cement. The difference in compressive strength between mixtures using the same production run of cement with and without FA throughout testing ranged between a minimum of 5.8% at 28-days and a maximum of 17.7% at 7 days. At extreme early ages, i.e., four and six hours, the difference in compressive strength was 10.1% and 9.8%. This is consistent with later ages, i.e., 56 days and 90 days, which had differences in compressive strength of 11.0% and 8.4%. The consistent difference implies that FA was inert, and therefore no pozzolanic activity occurred. PC 0.36 had less compressive strength throughout the testing period than all BCSA mixtures. Strength gain followed the same approximate trend as BCSA mixtures, although extreme early age compressive strength was not recorded for PC samples.

The compressive strength gain of concrete cylinders with w/cm=0.44 as a function of time is shown in Figure 25. BCSA 0.44-1 and BCSA 0.44-2 were cast using different production runs of BCSA cement. The cement used in BCSA 0.36-1 and 0.44-1 were from the same production run, and BCSA 0.36-2 and 0.44-2 were from the same production run. Unlike mixtures with w/cm=0.36, the difference in compressive strength between w/cm=0.44 mixtures made with different production runs is evident throughout the testing period. Like w/cm=0.36 mixtures, the largest difference in compressive strength between BCAS 0.44-1 and BCSA 0.44-2 occurs at extreme

early ages. At four and six hours, the difference in compressive strength is 21.3% and 19.4%, respectively. At later age, such as 90 days, the difference in compressive strength was 13.5%. It appears that the higher w/cm paired with the lower cement content, 485 kg/m$^3$ (682 lb/yd$^3$) did not negate any potential difference in cement reactivity due to age and production runs like in w/cm=0.36 mixtures.

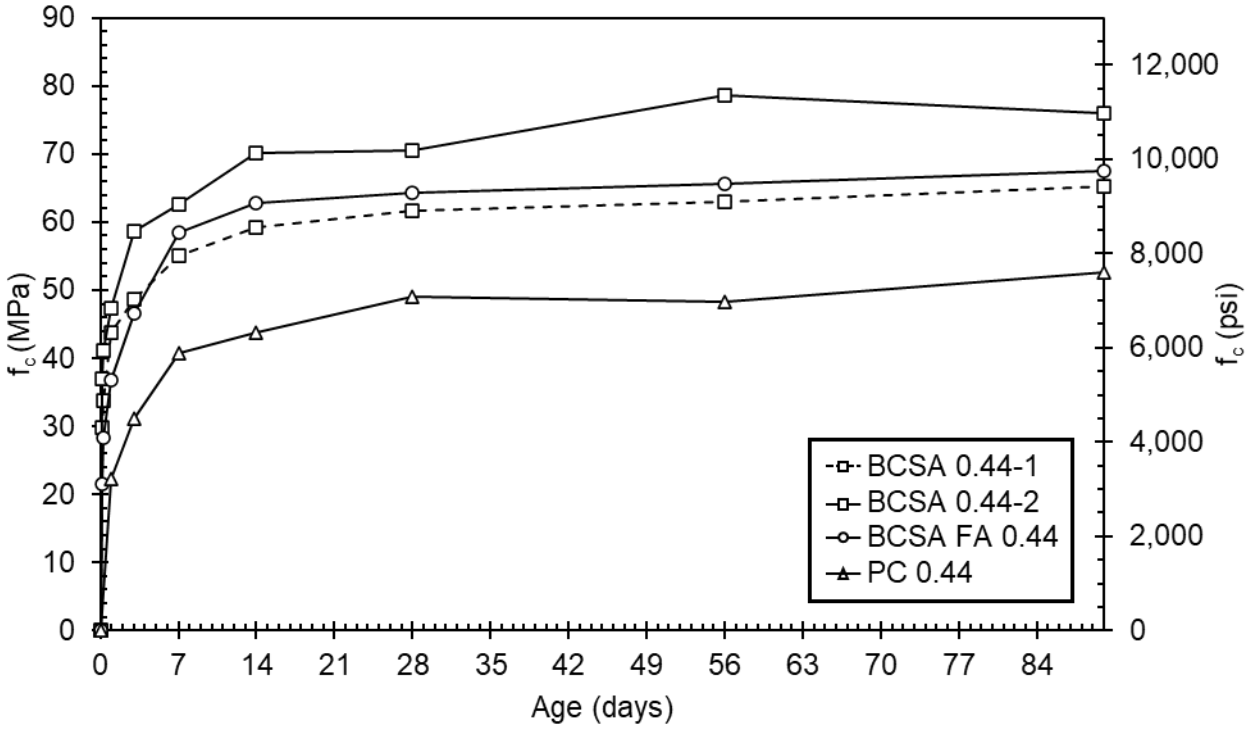


**Figure 25: Compressive strength gain for w/cm=0.44 mixtures**

BCSA FA 0.44 was cast using the same production run of BCSA 0.44-2. BCSA FA 0.44 shows the effect of a 15% cement replacement by FA and shows the effect of cement reactivity. Despite having a 15% cement replacement by FA, it has approximately equal compressive strength as BCSA 0.44-1 after three days. The difference in compressive strength between mixtures using the same production run of cement with and without FA throughout testing ranged between a minimum of 6.9% at seven days and a maximum of 53.4% at four hours. At extreme early ages, i.e., four and six hours, the difference in compressive strength was 53.4% and 37.1%. After seven days, the difference in compressive strength remains stable at approximately 12%. Like BCSA FA 0.36, it can be concluded that for BCSA FA 0.44, FA was inert, and therefore no pozzolanic activity occurred. PC 0.44 had less compressive strength throughout the testing period than all BCSA mixtures. Strength gain followed the same approximate trend as BCSA mixtures, although extreme early age compressive strength was not recorded for PC samples.

Figure 26 shows the bulk density results of all the ECC mixtures at 28 days. Notably, samples with 100% BCSA cement and varying OA replacement —55% and 70%—exhibited the highest and lowest densities, respectively. The variability in the graph appears to be within a normal range. The error bars, which represent the standard deviation or margin of error, are relatively small in relation to the overall density values for each mixture, suggesting minimal variability in the measured density values. This indicates consistent results across the samples tested. The density values follow a logical pattern based on the compositions, with minor fluctuations that could naturally occur due to material distribution or preparation differences. This result indicates

that higher OA content leads to a reduction in the overall density of the BCSA-ECC mixtures, likely due to the filler effect of OA (García-Maté et al., 2013), which has lower density compared to the cementitious materials it replaces. In summary, the densities for all mixtures are within a narrow range of approximately 210 to 220 kg/m³, which is typical for ECC materials(Game et al., 2022). The density values follow a logical pattern based on the compositions, with minor fluctuations that could naturally occur due to material distribution or preparation differences.

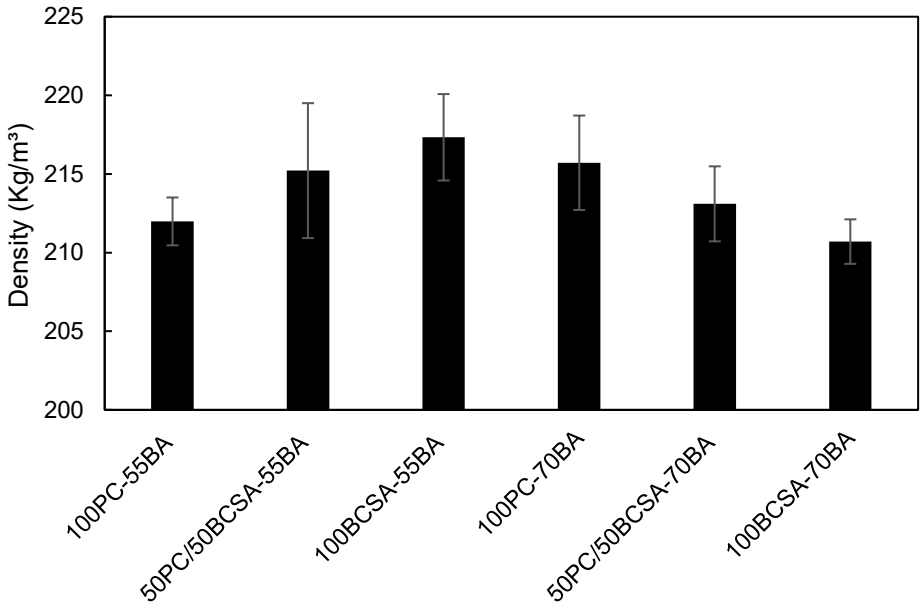


**Figure 26*:* Bulk Density of ECC Mixtures at 28 days**

## 4.5 Uniaxial Tensile Test

The tensile stress versus strain curves for various ECC mixtures at 28-days are detailed in Figure 27, a–f. The results indicate that all materials exhibited PSH behavior, with the 100BCSA and 100PC series demonstrating superior performance. Tensile properties such as first cracking strength, tensile strength, and tensile strain capacity are summarized in Figure 28, including values recorded for 1 and 7 days of curing.

Among the mixtures evaluated, the 100PC-70OA mixture exhibited the highest tensile strain capacity at early curing stages, achieving 4.94% at 1 day and 5.65% at 7 days. However, its strain capacity decreased to 2.09% by 28 days. In contrast, the 100BCSA-55OA mixture demonstrated better performance at later stages, with a strain capacity of 3.69% at 28 days, following initial values of 1.59% and 2.09% at 1 and 7 days, respectively. These findings indicate that increasing the OA content to 70% enhances the tensile strain capacity of ECC with 100% PC. However, for ECC with 100% BCSA, 55% OA replacement proves optimal.

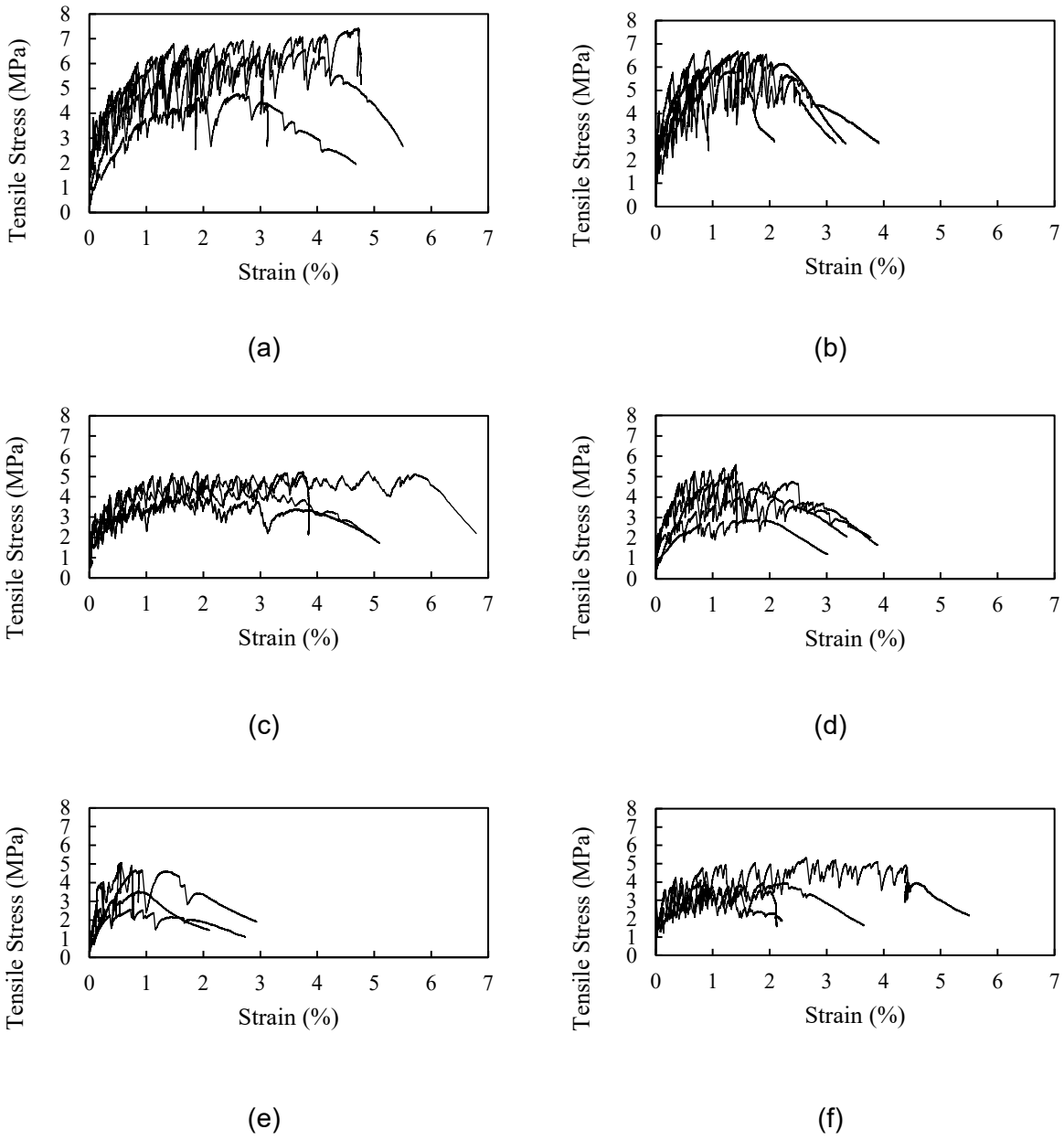


**Figure 27. Tensile Stress vs. Strain Curve for five replicate samples on each mixture design: (a) 100PC-55OA , (b) 50PC/50BCSA-55OA , (c) 100BCSA-55OA , (d) 100PC-70OA , e) 50PC/50BCSA-70OA , and (f) 100BCSA-70OA**

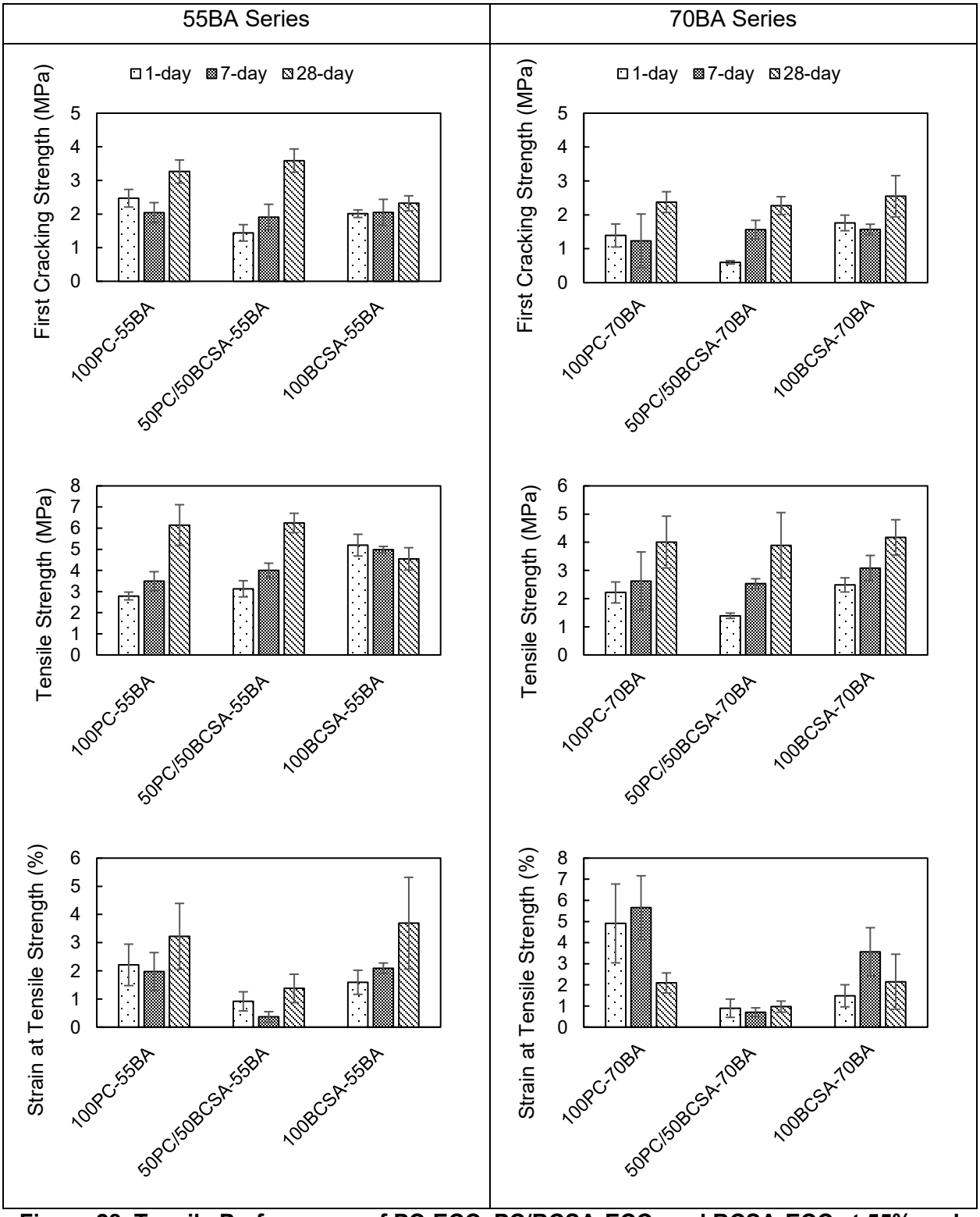


**Figure 28. Tensile Performance of PC-ECC, PC/BCSA-ECC, and BCSA-ECC at 55% and 70% Cement Replacement with OA**

Specimens with higher BCSA content, such as 100BCSA-55OA and 100BCSA-70OA, generally exhibited superior tensile strength and first cracking strength during the early curing stages (1-day and 7-day), highlighting the rapid strength-gain properties of BCSA. The 100BCSA-55OA mixture showed exceptional early performance, with tensile strengths of 5.20 MPa at 1 day, 4.98 MPa at 7 days, and 4.5 MPa at 28 days. These results underscore a trade-off between tensile strength and strain capacity, with different formulations offering varied performance profiles across curing intervals.

The 50BCSA/50PC-55OA mixture exhibited relatively low strain capacity and tensile strength across all curing periods, indicating more brittle behavior compared to other mixtures. Mixtures utilizing either 100% PC or 100% BCSA yield the most favorable tensile properties, while combining BCSA and PC does not produce optimal performance. Moreover, 100BCSA-55OA mixtures consistently show higher values of tensile strength compared to those with higher cement replacement with OA. This suggests that the 55% cement replacement with OA is more effective in enhancing tensile strength, highlighting the importance of careful material selection and proportioning to achieve superior mechanical properties.

The enhanced ductility in most ECC specimens with increasing quantities of OA can be explained by the micromechanics design concepts of ECC. To ensure robust strain-hardening behavior with multiple micro-cracking, an adequate margin between the complementary energy of the fiber-bridging relation ($J_b'$) and the matrix crack tip toughness ($J_{tip}$) is required (Li, n.d.; Noorvand et al., 2019). Therefore, a large $J_b'/J_{tip}$ ratio, also known as the PSH energy index, favors saturated multiple cracking.

Conversely, the low ductility of ECC materials with 50PC/50BCSA can be attributed to the combined effect of increasing $J_{tip}$ and decreasing $J_b'$, leading to a reduced PSH energy index. An increase in OA content reduces $J_{tip}$, due to lower reactivity, and increases $J_b'$, enhancing the PSH energy index (Li, 2019; Savadogo et al., 2024). However, this increase in OA content is also associated with a decrease in the fiber-bridging capacity ($\sigma_0$) of ECC materials, resulting in reduced tensile strength. Furthermore, the tensile strain capacity observed in ECC with 100% BCSA is linked to a rise in $\sigma_0$, which enhances tensile strength by effectively transferring loads and controlling crack propagation (Li, 2019). The dense formation and needle-like characteristics of the hydration product, specifically ettringite crystals (García-Maté et al., 2013), are hypothesized to enhance the bond between the matrix and fiber.

The blend of PC and BCSA cement improves the tensile strength at later ages (28-day period). Literature indicates that the utilization of 12% PC in the CSA-containing cement blend used in the ECC helped to enhance tensile strength at 28 days (Jiang et al., 2023). Hence, more studies are needed to elucidate how a small and large percentage of PC replacement with BCSA cement affects the tensile properties of ECCs. It is important to note that the documented results cover the early to medium-term curing periods (1-28 days), and the long-term effects could vary.

The findings demonstrate that BCSA-ECCs exhibit superior early-age tensile strength when BCSA cement is used either as a partial or complete replacement for PC. Specifically, the 100BCSA-55OA mixture showed the highest tensile strength at early curing stages, highlighting BCSA cement's rapid strength-gain properties. Additionally, using OA as an alternative SCM at 55% cement replacement with OA of total cementitious materials showed comparable tensile properties to PC-ECCs. These results suggest that BCSA-ECCs are particularly beneficial for applications requiring quick setting and high early strength, such as pavement repairs, precast elements, and fast-track construction projects. By incorporating BCSA-ECCs, the construction industry can reduce their dependency on traditional PC and FA.

## 4.6 Crack Analysis

The results in Table 8 represent the average crack width (in micrometers) of ECC specimens after a uniaxial tensile test. For ECC, smaller crack widths are desirable as they minimize the penetration and diffusion of aggressive ions (e.g., chlorides, sulfates), thus enhancing the structure's durability. A crack width below 100 μm is considered effective in preventing ion ingress, significantly extending the lifespan of ECC structures (Li, 2019). The best-performing mixture is 100BCSA-55OA with an average crack width of 38.90 μm. This value is below the typical 45 μm crack width associated with saturated cracking patterns in ECC, as seen in Table 8, indicates excellent control of crack width, likely due to effective fiber-matrix interaction (Li, 2019).The second-best performance is observed in 100BCSA-70OA (43.97 μm), which is also well below the 100 μm threshold and within the typical range for ECCs. The worst-performing mixture in terms of crack width is 50PC/50BCSA-55OA, with an average of 111 μm, exceeding the 100 μm threshold. This indicates reduced crack control, possibly due to the interaction between fibers and the cementitious matrix being less effective in this composition.

Mixtures with 100% BCSA, particularly 100BCSA-55OA (SD = 6.07) and 100BCSA-70OA (SD = 15.21), exhibit relatively low variability, indicating consistent crack width control across samples. 50PC/50BCSA-55OA shows the highest variability (SD = 36.90), suggesting inconsistencies in material distribution or fiber alignment, which may have contributed to its poorer average crack width performance.

**Table 7. Crack pattern of ECCs mixtures**

| Age | 100PC-55OA | 50BCSA/50PC-55OA | 100BCSA-55OA | 100PC-2.3OA | 50BCSA/50PC-2.3OA | 100BCSA-2.3OA |
|---|---|---|---|---|---|---|
| 1-day | 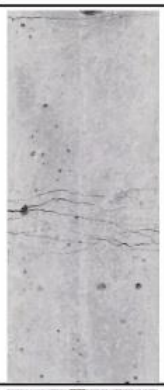 |  |  |  | 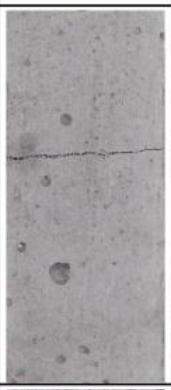 |  |
| 7-day |  |  |  |  |  |  |
| 28-day |  |  |  |  |  |  |

The effect of OA is explained as follows: at 55% OA replacement, the 100% BCSA mixture significantly outperforms both 100% PC and the 50PC/50BCSA combination, highlighting the effectiveness of BCSA cement in reducing crack widths. At 70% OA replacement, the trend is similar, with 100BCSA mixtures maintaining better crack control than mixtures with PC or a PC/BCSA combination. Smaller crack widths, particularly in the 100BCSA mixtures, indicate effective flat crack propagation and multiple microcracking (Li, 2019). It is hypothesized that these properties result from strong fiber-matrix bonding, which allows fibers to bridge cracks effectively while redistributing tensile stresses. The larger crack widths in the 50PC/50BCSA mixtures suggest less effective stress transfer, potentially due to weaker interfacial bonding or uneven fiber orientation and distribution.

**Table 8. Average crack width of ECC after Uniaxial Tensile Test**

| Specimen | ϖ 1 (μm) | ϖ 2 (μm) | ϖ 3 (μm) | ϖ 4 (μm) | ϖ 5 (μm) | Average (μm) | SD (μm) |
|---|---|---|---|---|---|---|---|
| 100PC-55OA | 80.41 | 84.60 | 59.90 | 67.06 | 81.99 | 74.79 | 10.74 |
| 50PC/50BCSA-55OA | 85.92 | 80.25 | 122.81 | 96.75 | 170.40 | 111.23 | 36.90 |
| 100BCSA-55OA | 34.02 | 35.77 | 44.74 | 33.93 | 46.32 | 38.96 | 6.07 |
| 100PC-70OA | 46.57 | 50.54 | 49.78 | 60.12 | 51.31 | 51.66 | 5.06 |
| 50PC/50BCSA-70OA | 101.88 | 86.18 | 71.40 | 111.23 | 91.18 | 92.37 | 15.21 |
| 100BCSA-70OA | 26.12 | 38.30 | 38.91 | 49.83 | 66.68 | 43.97 | 15.22 |

ϖ: crack width

## 4.7 Flexural Test

Figure 29 presents the flexural stress vs. deflection curves for the best-performing ECC mixture, 100BCSA-55OA, at 28 days. As expected, the ductile tensile behavior of 100BCSA-55OA is reflected in its flexural performance, showing a pseudo strain-hardening behavior after the first-cracking strength is reached. This behavior allows significant deformation while increasing load-carrying capacity. The curves exhibit three distinct regions:

- Elastic Region: At low deflections (0–1 mm), the curves rise steeply, showing a linear elastic response to the applied load.
- Maximum or peak Strength: Around 8–11 MPa, the curves reach their peak, indicating the first cracking strength or maximum load capacity.
- Post-Peak Region: After the peak, the curves show a gradual decline in stress, corresponding to post-cracking behavior. Multiple cracks are generated in the ECC material, with fibers bridging these cracks to sustain the load. Over large deflections (~4–8 mm), the curves demonstrate deflection-hardening behavior, as the material retains significant load-bearing capacity, indicating excellent ductility and energy absorption capacity (toughness). Eventually, fibers rupture or pull out, leading to deterioration.

At 28 days of curing, the flexural strength of 100BCSA-55OA was 10.51 MPa, approximately twice that of regular concrete, and similar to PC-based ECC in literature (Gabriel Arce et al., 2019; 2018; Noorvand et al., 2019). Table 9 further summarizes the first-cracking strength, flexural strength, and deflection capacity. Figure 30 illustrates the crack development in 100BCSA-55OA ECC material following a flexural test. The left panel presents a larger view of three beam specimens, labeled 1, 2, and 3 (replicates), each showing visible cracks extending along their lengths. On the right, three corresponding close-up images provide detailed views of the cracks for each specimen, highlighting their irregular propagation and surface texture. The cracks extend vertically through the material, indicating failure and deformation under flexural stress. A ruler at the bottom of each close-up offers a scale for measuring the crack size and extent. This figure visually illustrates the behavior of the ECC material under flexural load, showcasing the development and progression of cracks.

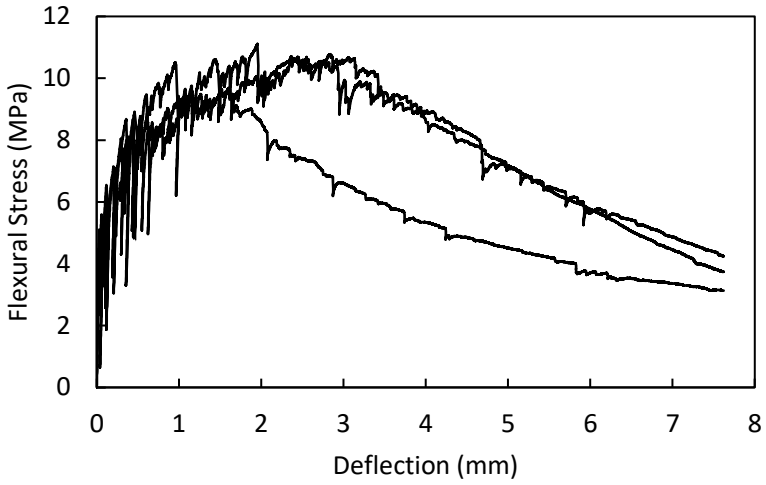


**Figure 29. Flexural stress vs. deflection curves**

**Table 9. First-cracking strength, flexural strength, and deflection capacity of 100CSA-55OA ECC**

| Specimen | First-Cracking Strength (MPa) | Flexural Strength (MPa) | Deflection Capacity (mm) |
|---|---|---|---|
| 1 | 5.11 | 9.64 | 1.52 |
| 2 | 4.55 | 11.11 | 1.95 |
| 3 | 5.60 | 10.78 | 2.85 |
| Average | 5.09 | 10.51 | 2.11 |
| SD | 0.53 | 0.77 | 0.68 |

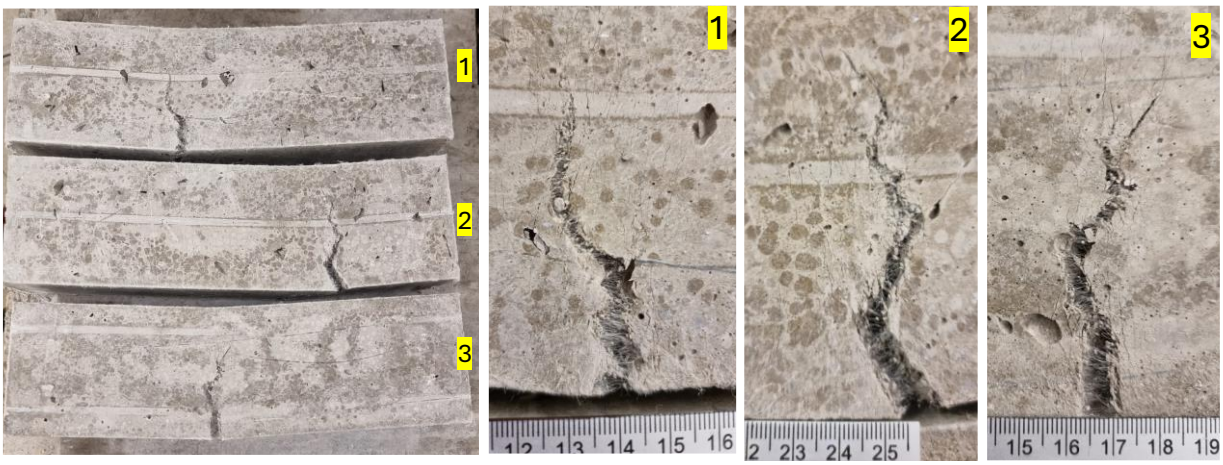


**Figure 30. Crack development of 100BCSA-55OA ECC after flexural test.**

## 4.8 Ultrasonic Pulse Velocity (UPV)

UPV measurements were used to establish a relationship between compressive strength and UPV for the concrete mixtures in the corrosion portion of this study. Figure 31 shows the relationship between $f_c$ and UPV for all BCSA cement-based mixtures with respect to time. At later ages (indicated by darker marker fill in Figure 31), both $f_c$ and UPV increase. UPV decreases due to a less dense microstructure, or a microstructure with abundant air voids or microcracking. UPV increases as the material densifies, so it can be concluded that the microstructure is increasing in density as time increases. A denser microstructure will also generally coincide with increased $f_c$. The rate at which $f_c$ increases compared to the rate at which UPV increases must be established to accurately estimate $f_c$ based on UPV.

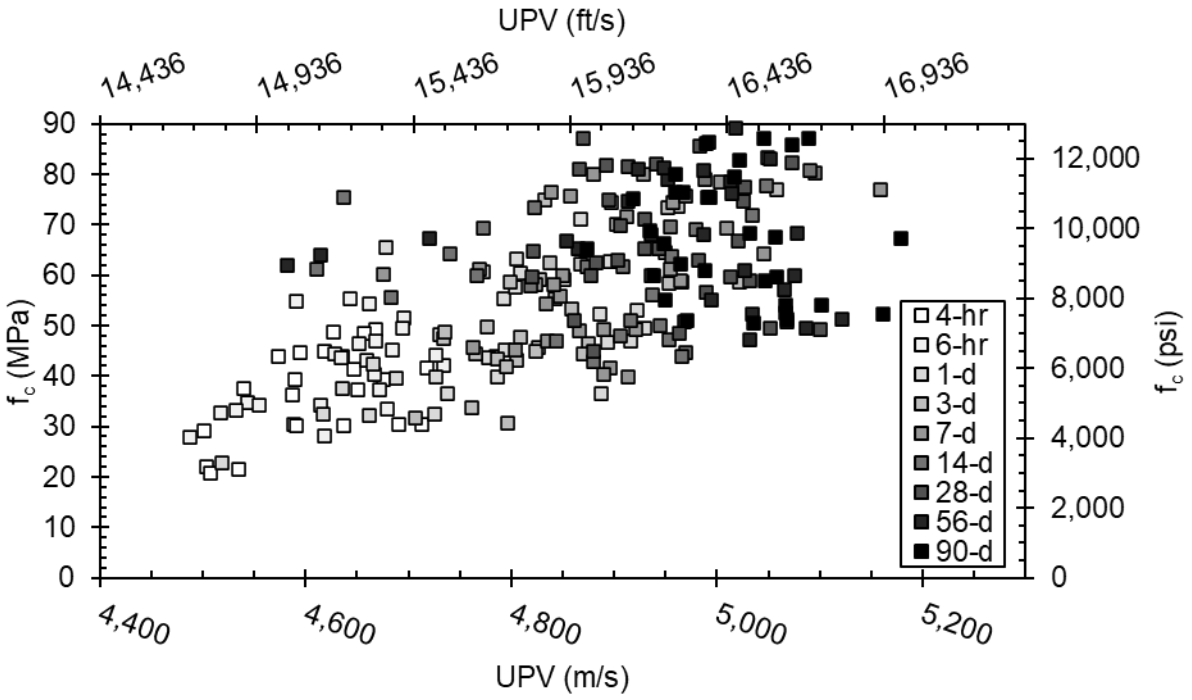


**Figure 31: Relationship between $f_c$ and UPV with time**

Best fit lines were fit to all BCSA mixtures using the same w/cm at all ages. An exponential relationship, such as the one described in Equation 1 yielded coefficients listed in

Table 10. The coefficient A, which relates to the aggregate type and sand to coarse aggregate ratio (S/A) is different by an order of magnitude for each w/cm. S/A for the w/cm=0.36 and 0.44 mixtures were 0.34 and 0.38, respectively. Since the same sand and coarse aggregate were used in the different mixtures, it can be concluded that the 0.04 increase in S/A resulted in the decrease in an order of magnitude of the A coefficient.

**Table 10: Coefficients for $f_c$-UPV equation**

| w/cm | A | B |
|---|---|---|
| 0.36 | 0.171 | 0.001 |
| 0.44 | 0.016 | 0.002 |

Predicted values of $f_c$ based on measured UPV values can be calculated by substituting the coefficients A and B into Equation 1. The resulting predicted $f_c$ compared to actual $f_c$ are shown in Figure 32. Predicted values were calculated with the prediction equation corresponding to the same w/cm as the mixture. A line of equality representing perfect agreement between predicted and actual values is included in Figure 32. The distance between plotted values and the line of equality represents residuals, or the distance between expected and actual values. Smaller distances between plotted values and the line of equality indicate good agreement with the prediction equation, and larger distances indicate poor agreeance with the prediction equation.

At early ages, specifically at ages less than three days, residuals appear smaller than at later ages. It also appears that predicted $f_c$ are more likely to be over estimations at earlier ages. At later ages, residuals appear larger and consistently underestimate $f_c$ based on the greater number of values below the line of equality.

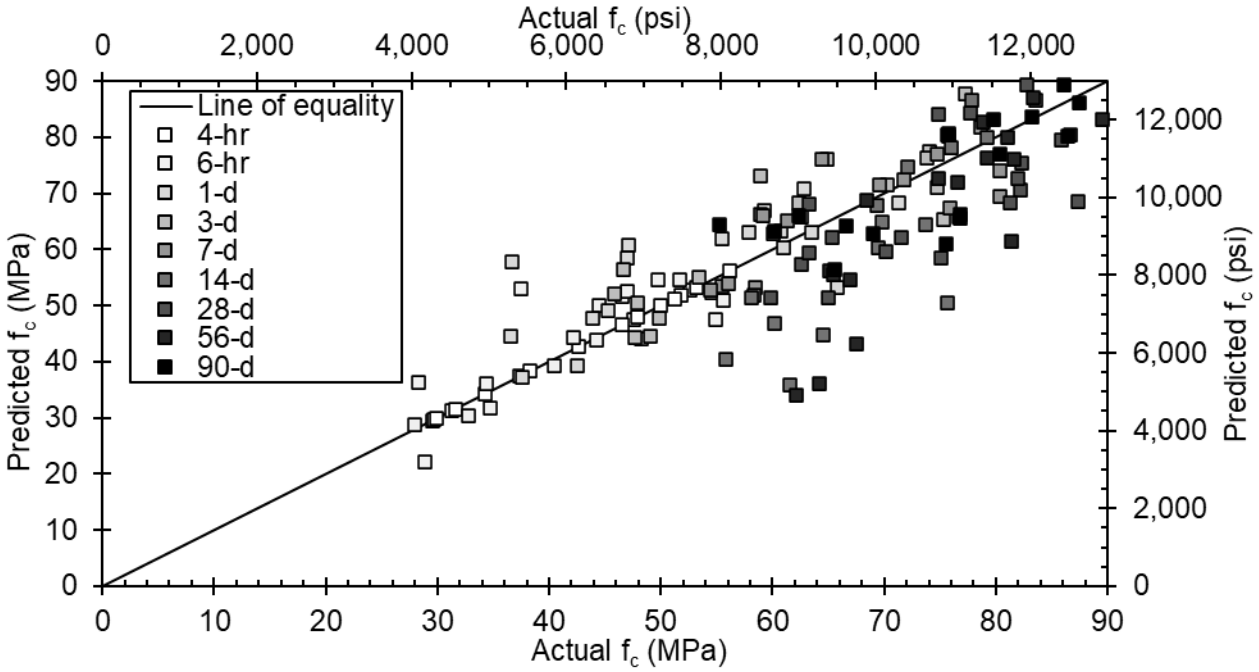


**Figure 32: Relationship between actual and predicted $f_c$ based on UPV**

## 4.9 Corrosion Tests

ASTM G109 specifies a standard cover depth based on aggregate size and specifies 28 days moist curing time prior to exposure to chlorides. The cover depth based on the aggregate size used in this research was 25 mm (1 in.). Figure 33 shows the results of this standard testing condition for BCSA cement and PC specimens. The inset graph in Figure 33 includes the entire range of TC for BCSA 0.44-1 and 0.36-1. While both BCSA specimen sets exceeded the 150 coulomb TC limit five weeks after saltwater exposure, BCSA 0.44-1 had higher TC throughout testing. At the end of testing, BCSA 0.44-1 had more than four times greater TC than BCSA 0.36-1, indicating that the more dense microstructure found in mixtures with lower w/cm may aid in the passivation and protection of reinforcing steel from corrosion. Both PC specimens remained below the 150 coulomb TC limit throughout the testing period.

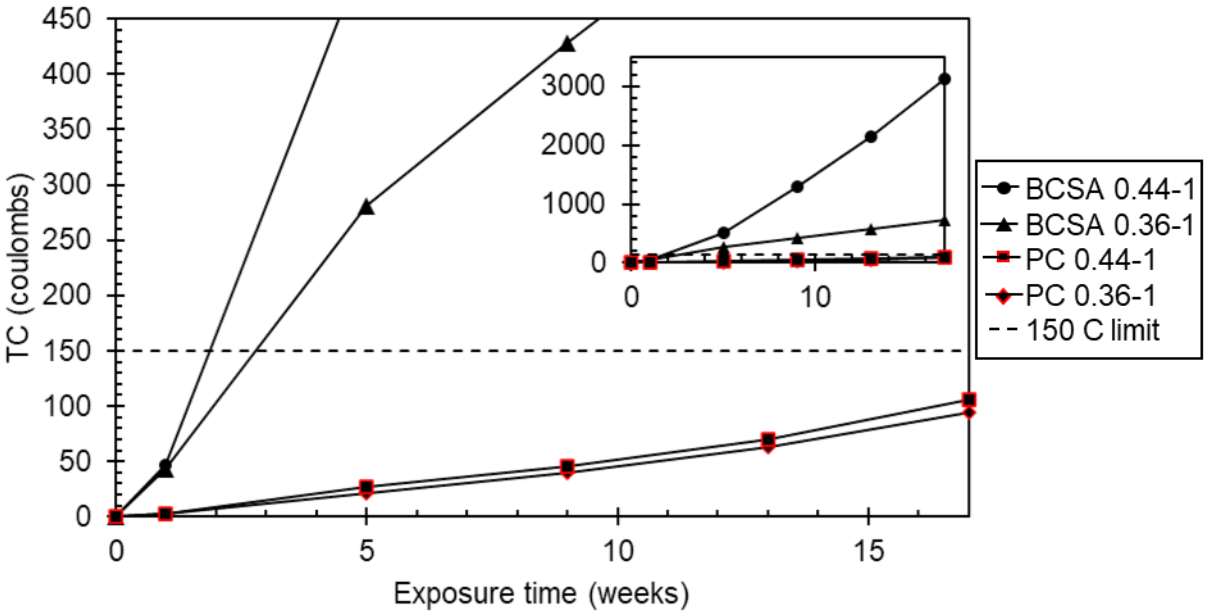


**Figure 33: Total corrosion for specimens with 25 mm (1 in.) cover depth and 28-day moist cure time**

It was expected that BCSA specimens moist cured for 28 days would not perform as well as PC specimens. Since initial pore solution pH of BCSA cement concrete is 11-12 and corrosion can occur at pH as high as 11.5, reinforcing steel in BCSA cement concrete may be more at risk for corrosion than PC concrete. After 28 days of moist curing, the compound which comprises approximately 45% of BCSA cement by mass, belite, may not have sufficient curing time to complete the hydration process yet. Without this densification of the microstructure of BSCA cement concrete rapid chloride ingress occurred, resulting in a rapid increase in TC.

After the TC of specimens passed 150 coulombs, they were cut apart to investigate the pH of the pore solution of the concrete and to visually inspect rebar for any signs of corrosion. A cut apart BCSA 0.44-1 specimen is shown in Figure 34. Brown surface rust was prevalent along the length of the exposed rebar section. An area of pitted corrosion, outlined by a black box, is evident and a corrosive stain is visible on the concrete section which was in contact with it, also outlined by a black box. pH indicator spray was applied to the cut section, revealing a pH between 8-10 throughout the section, excluding coarse aggregates.

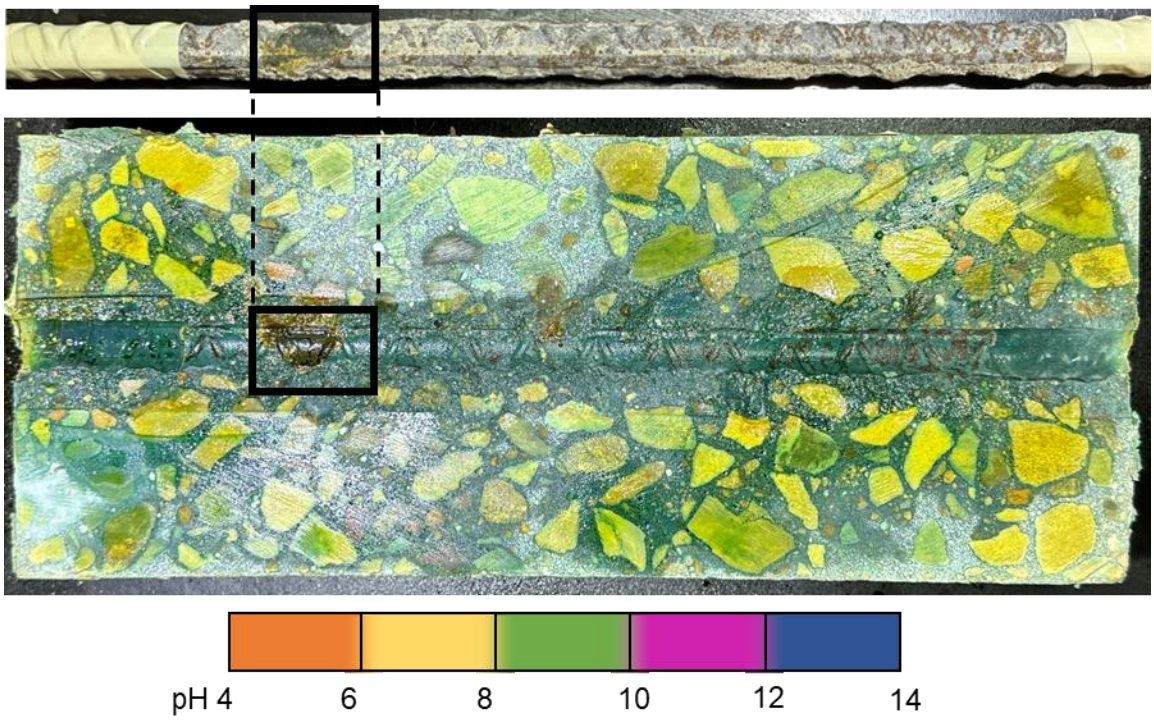


**Figure 34: BCSA 0.44-1, 25 mm (1 in.), 28-d rebar investigation after failure and pH indicator spray on concrete**

A cut apart BCSA 0.36-1 specimen is shown in Figure 35. Brown surface rust was evident along the length of the exposed rebar section but was not as prevalent as in BCSA 0.44-1. No areas of pitted corrosion are visible. pH indicator spray was applied to the cut section, revealing a pH between 10-12 throughout the section, excluding coarse aggregates. The area directly in contact with rebar had a pH between 12-14. The increased pH immediately surrounding the rebar is an indication of passivation. Although passivation may have occurred, it may not have occurred to a great enough extent to protect the rebar from the formation of brown rust or may not have occurred before the initial saltwater exposure.

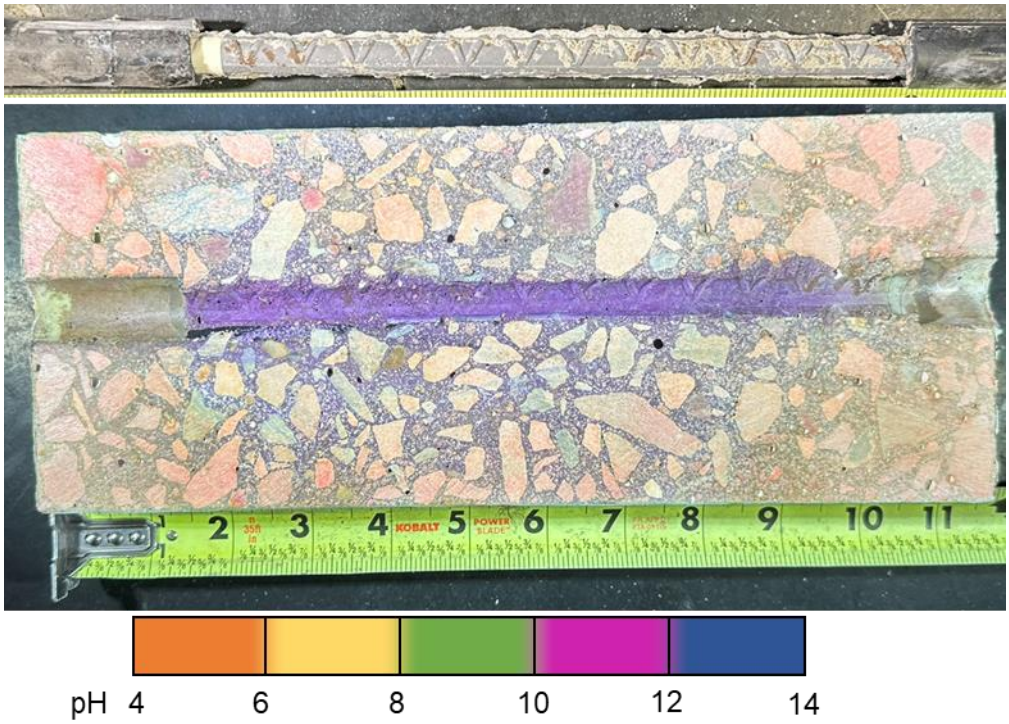


**Figure 35: BCSA 0.36-1, 25 mm (1 in.), 28-d rebar investigation after failure and pH indicator spray on concrete (note: 25.4 mm=1 in.)**

A cut apart PC 0.36 sample is shown in Figure 36. No brown surface rust is visible on the rebar. The entire concrete section has a pore solution pH of 12-14 except coarse aggregates. This result provides a direct comparison with BCSA cement based specimens. Since the pH indicator spray lacks the precision to differentiate pH between 12-14, the extent of passivation cannot be determined. It can be concluded, though, that either the pore solution pH or passivation was adequate to protect reinforcing steel in PC specimens throughout the testing period.

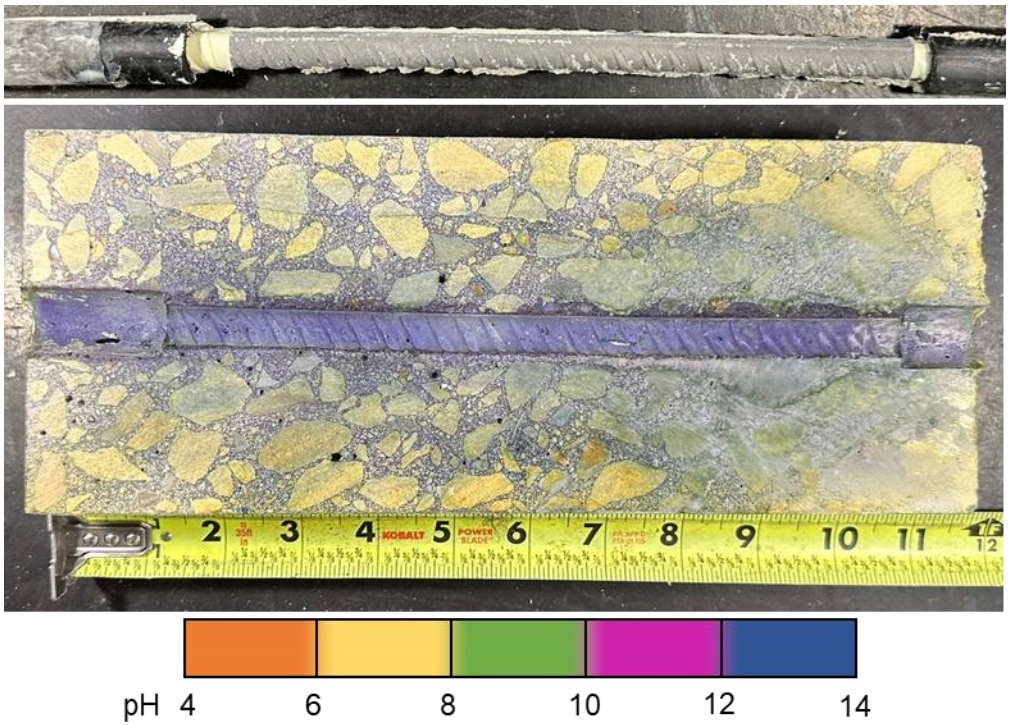


**Figure 36: PC 0.36, 25 mm (1 in.), 28-d rebar investigation after testing period and pH indicator spray on concrete (note: 25.4 mm=1 in.)**

Generally, approximately 80% of compressive strength gain of BCSA cement concrete has occurred at seven days. Seven days, therefore, is approximately analogous to 28-day strength in PC concrete in terms of the extent of strength gain. Figure 37 includes the TC results for BCSA 0.44-2 and 0.36-2, both cast with 25 mm (1 in.) cover depth and seven days moist cure time. PC 0.36-1 with 25 mm (1 in.) cover depth and 28 days moist cure time is also included in Figure 37. While seven days moist cure time for BCSA cement-based specimens may be an adequate analogy for the gain in compressive strength to 28 days moist cure time for PC, it is not an analogous "age" for the protection and passivation of reinforcing steel. Additionally, the gain in compressive strength should not serve as an indicator of reinforcing steel protection and passivation.

The BCSA cement specimens in Figure 33 are cast with a different production run of BCSA cement than specimens described in Figure 37. Potential differences in cement reactivity may be the cause of lower TC values with specimens moist cured for seven days than specimens moist cured for 28 days. Similar to the compressive strength results, little difference was observed between the results of the mixtures cast at a w/cm=0.36 but with different production runs of cement. A greater difference was observed between the results of mixtures cast with w/cm=0.44 from different cement production runs.

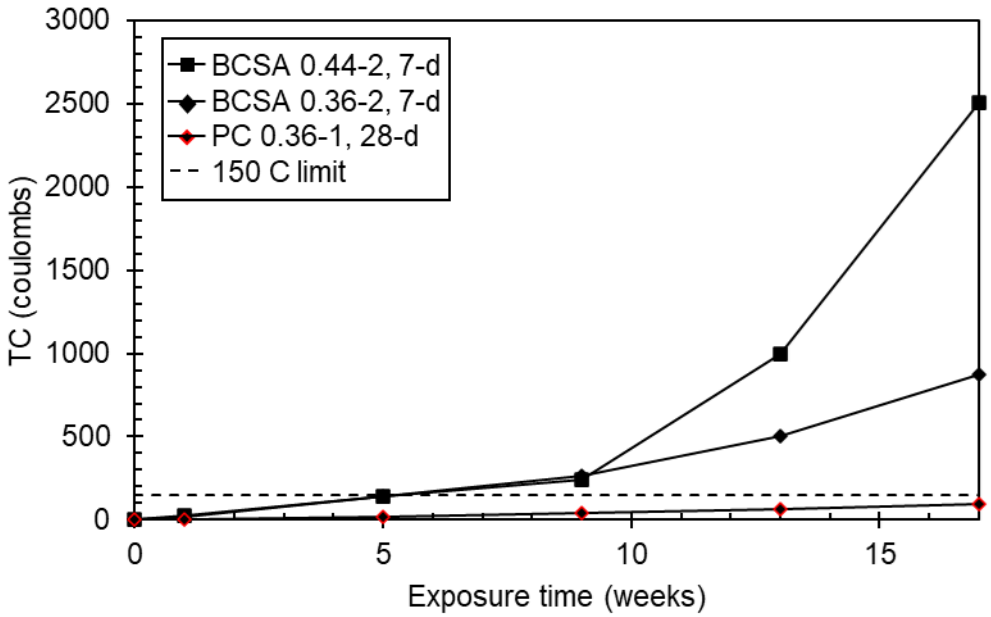


**Figure 37: Total corrosion for specimens with 25 mm (1 in.) cover depth and variable moist cure time**

In ACI 318-19, cover depths are increased for structural members that are exposed to weather or are in contact with the ground. Theoretically, different cementitious systems could require different cover depths based on their microstructural properties. Figure 38 includes results for both BCSA w/cm with cover depths of 38 mm (1.5 in.) and 51 mm (2 in.) for mixtures subjected to a 28-day moist cure time. Increasing the distance which chlorides had to travel to reach reinforcing steel was effective in slowing the rate of corrosion for both w/cm. Both BCSA 0.44-2 cover depths exceeded the 150 coulomb limit defined as a specimen failure after nine weeks of saltwater exposure, but increasing cover depth decreased the value of TC at the end of the testing period. BCSA 0.36-2 with 38 mm (1.5 in.) cover depth exceeded the 150 coulomb limit after 13 weeks of saltwater exposure and BCSA 0.36-2 with 51 mm (2 in.) cover depth exceeded the limit after 17 weeks of exposure. The increased cover depth marginally improved the rate of corrosion initiation.

While all specimens exceeded the 150 coulomb limit before the end of the testing period, time to corrosion was extended with increased cover depth. Combining increased cover depth and decreased w/cm was most effective in extending the time to corrosion for specimens moist cured for 28 days.

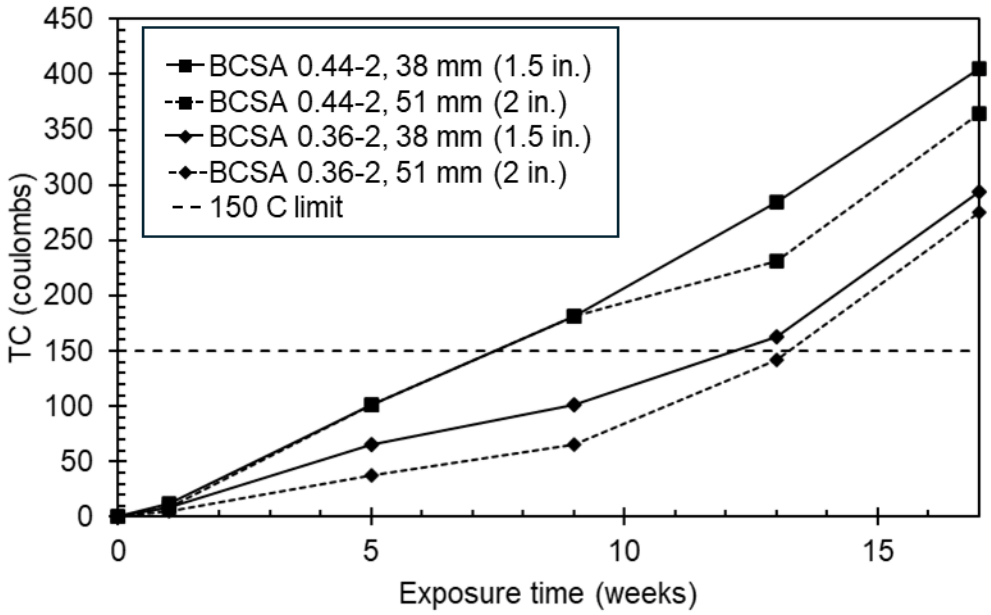


**Figure 38: Total corrosion for specimens with variable cover depth and 28 day moist cure time**

Increasing moist curing time increases the water available to react with the belite in BCSA cement at later ages. Belite is a slow reacting cement compound and would be expected to take several months to hydrate. The hydration of belite creates additional hydration products which contribute to a more dense microstructure. Figure 39 includes results for both BCSA w/cm and increased cover depths to 38 mm (1.5 in.) and 51 mm (2 in.) with 90 day moist curing time. Increasing the distance which chlorides had to travel through a more dense microstructure to reach reinforcing steel was effective in slowing the rate of corrosion for both w/cm. BCSA 0.44-2 cover depths exceeded the 150 coulomb limit to define specimen failure, but was delayed to 13 and 17 weeks saltwater exposure. Neither BCSA 0.36-2 cover depth exceeded the 150 coulomb limit during the testing period.

Since neither BCSA 0.36-2 cover depth with 90 day moist cure time exceeded the TC limit, it can be concluded that the combination of decreasing w/cm, increasing cover depth, and increasing moist curing time were effective to protect reinforcing steel. While BCSA 0.44-2 with 51 mm (2 in.) cover depth exceeded the 150 coulomb limit after 17 weeks of saltwater exposure, its final TC value was near 150 coulombs, indicating that corrosion protection may be possible at higher w/cm provided cover depths are greater than 51 mm (2 in.) or moist curing time is longer than 90 days.

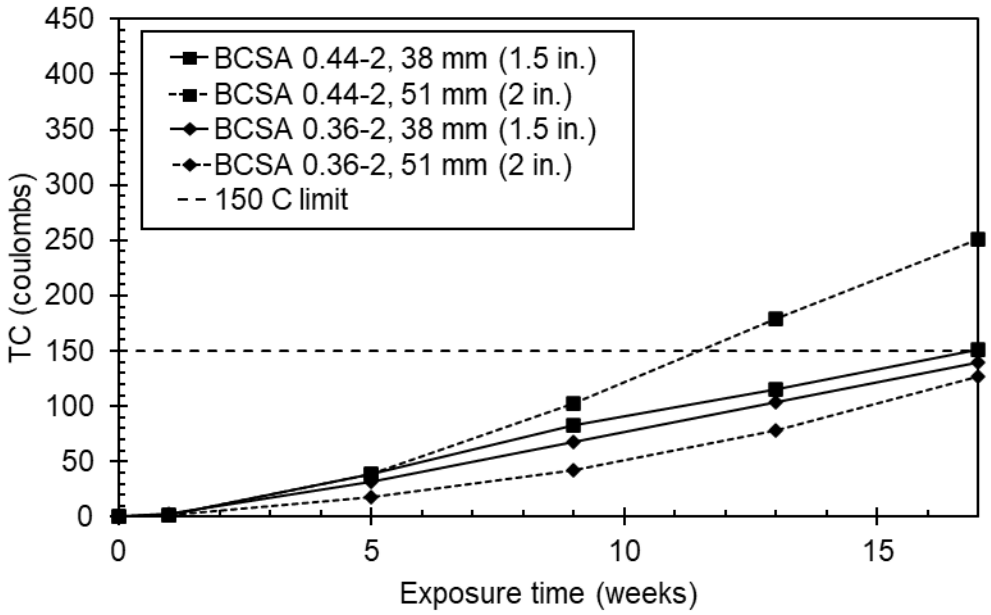


**Figure 39: Total corrosion for specimens with variable cover depth and 90 day moist cure time**

Increasing cover depth may not always be a practical solution to protect reinforcing steel. A common hydrophobic concrete sealant, silane, was applied to the surface of the integral dam to evaluate the effectiveness of surface treatments at impeding chloride ingress. Figure 40 includes results for both BCSA w/cm with 25 mm (1 in.) cover depth and 90 day moist cure time. The inset graph in Figure 40 reveals the extent of TC for BCSA 0.44-1. These specimens were made with the older and less reactive production run of BCSA cement. One specimen set for each w/cm has a silane surface treatment prior to the first ponding cycle. BCSA 0.44-1 and BCSA 0.36-1 without any surface treatment exceeded the 150 coulomb limit after nine and 17 weeks of saltwater exposure. The specimen sets that received the silane surface treatment did not exceed the 150 coulomb limit during the testing period.

Since neither specimen set that received the silane surface treatment with 90 day moist cure time and 25 mm (1 in.) cover depth exceeded the TC limit, it can be concluded that the silane surface treatment is effective to protect reinforcing steel. Unlike the specimens cast from BCSA 0.36-2 and 0.44-2 which also moist cured for 90 days, the specimens sets cast from BCSA 0.36-1 and 0.44-1 exceeded the TC limit. Exceeding the TC limit may be attributed to the reduced cover depth or differences in cement reactivity.

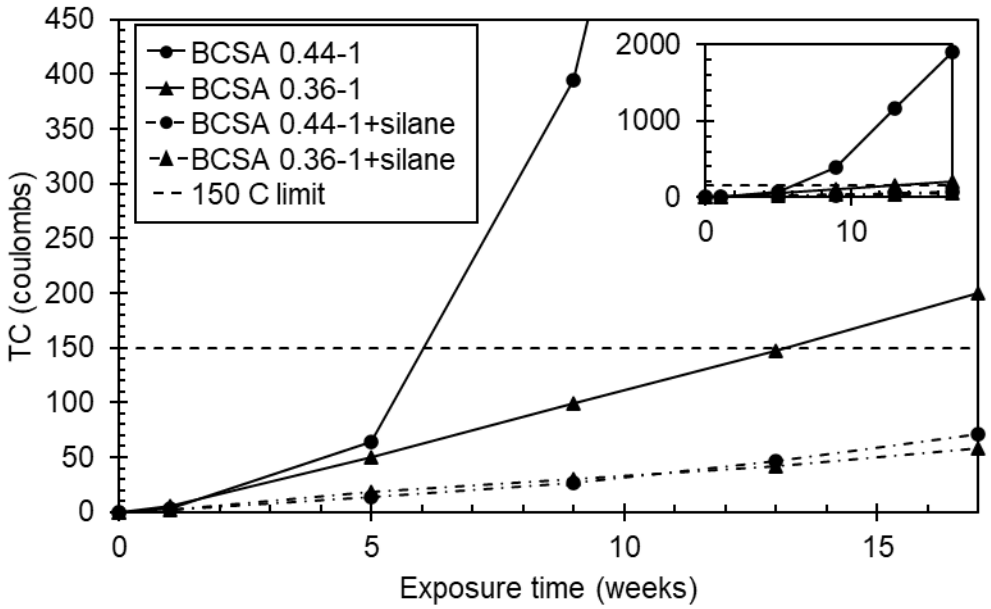


**Figure 40: Total corrosion for specimens with 25 mm (1 in.) cover depth, 90 day moist cure time and silane surface treatment**

Another potential reinforcing steel protective meausre evaluated was the partial cement replacement with Class C FA and 25 mm (1 in.) cover depth. Figure 41 compares the results for both BCSA FA w/cm with 38 mm (1.5 in.) cover depth. All specimens had 90 day moist cure time. Unlike other specimen sets, the lower w/cm (0.36) performed worse than the higher w/cm (0.44). BCSA FA 0.36 exceeded the TC limit after 13 weeks of exposure. The TC values for BCSA 0.44 FA follow a similar trend as BCSA 0.44-2 with 38 mm (1.5 in.) cover depth. Since FA replacements did not have consistent results with both w/cm, no general conclusions may be drawn regarding the effectiveness of FA. At higher w/cm=0.44, the inclusion of FA yielded similar TC results as increasing cover depth by 12.5 mm (0.5 in.).

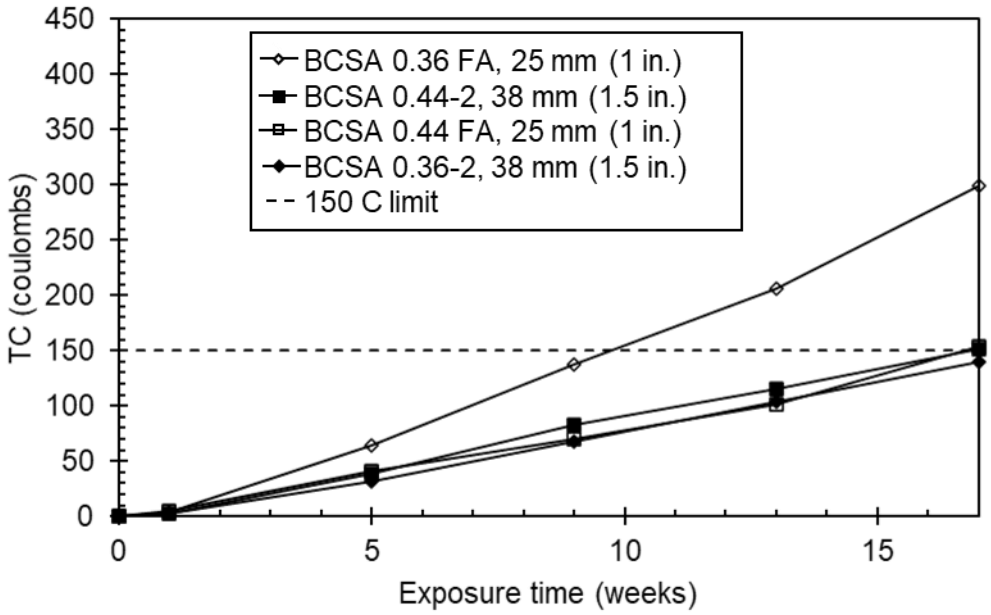


**Figure 41: Total corrosion comparing the effect of FA compared to increased cover depth**

Four specimen sets did not exceed the TC limit throughout the testing period. Figure 42 includes the TC results for two BCSA 0.36-2 specimen sets: 38 mm (1.5 in) and 51 mm (2 in.) cover depth, the PC control specimens, BCSA 0.44-1+silane and BCSA 0.36-1+silane. All BCSA specimen sets which did not exceed the TC limit were moist cured for 90 days. The silane surface treatment specimens had the lowest TC at the end of the testing period. This indicates that silane is an effective surface treatment to protect reinforcing steel in BCSA cement concrete from corrosion. But the application of silane prevents all moisture from penetrating the surface which it is applied to. Using a lower w/cm, increasing cover depth, and extending the moist curing time was also effective in protecting reinforcing steel in BCSA cement concrete.

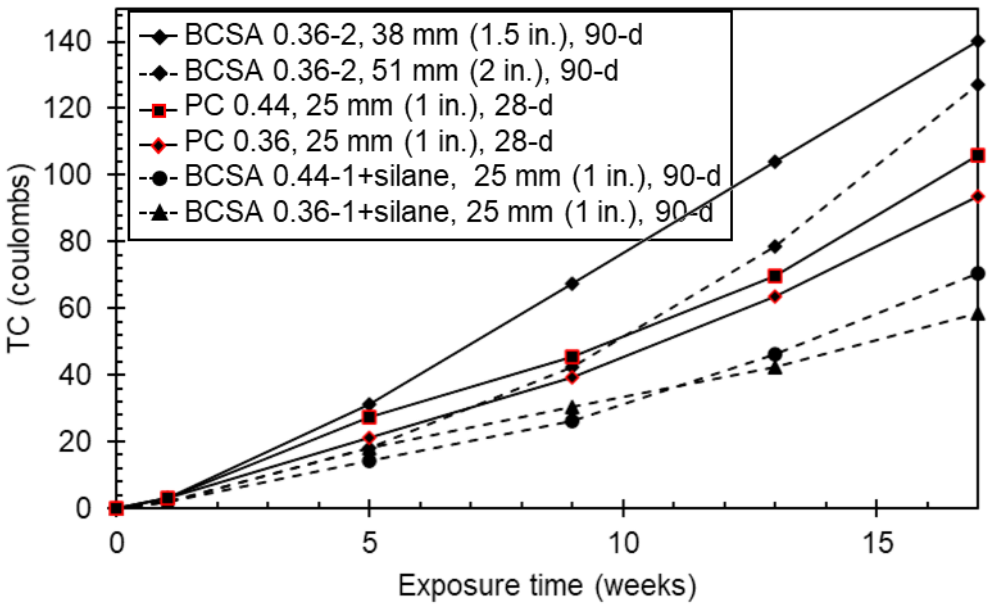


**Figure 42: Total corrosion for specimens which did not exceed the TC limit during the testing period**

# Chapter 5. Conclusions and Recommendations

This study investigated the use of BCSA cement as a partial or complete replacement for PC in ECC, focusing on flowability, setting properties, and mechanical performance at 1, 7, and 28 days. ECC mixtures incorporating varying levels of BCSA (0, 50, and 100%), along with the effect of OA at two cement replacement levels of 55% and 70% were evaluated. This study also investigated the durability properties of BCSA cement concrete in terms of reinforcement corrosion. BCSA cement concrete specimens with varying w/cm, cover depths, moist curing times, and protective measures were evaluated and compared to standard PC specimens. The compressive strengths of all mixtures and predicted compressive strength of BCSA mixtures were evaluated.

The findings are summarized as follows, starting with the BCSA ECC study:

- ECC with 100% BCSA demonstrated flowability comparable to those with lower BCSA percentages and 100% PC. The addition of BCSA significantly accelerated setting times, while higher OA content extended the setting times. This behavior is attributed to the chemistry of BCSA which promotes the formation of ettringite and thereby enhances early strength.
- The highest compressive strength at 28 days (48 MPa) was observed in the 50% BCSA replacement mixture, indicating an optimal balance of constituents for compressive strength performance, though it exhibited a poor tensile behavior caused by high $J_{tip}$ and low $J_b'$.
- Specimens with 100% BCSA and lower OA content showed significant early-age strength gains due to rapid hydration and ettringite formation. In contrast, mixtures containing PC exhibited substantial relative strength gains over time, suggesting that PC promotes hydration through secondary reactions with OA at later ages.
- Mixtures with BCSA, particularly those with 100% BCSA and high OA content, displayed lower long-term strength, likely due to the diluting effect of OA on key hydration phases such as anhydrite and belite.
- All mixtures composed entirely of BCSA cement demonstrated promising PSH behaviors. Notably, the mixture with 100% BCSA cement at 55% cement replacement with OA achieved the highest tensile strain capacity, reaching 3.69% at 28 days. While increasing the cement replacement with OA from 55% to 70% demonstrated a positive effect on the tensile strain capacity of ECC when using 100% PC.
- However, for ECC using 100% BCSA, the optimal OA content was found to be 55%. The higher ductility in ECC specimens with increasing OA content in PC-OA based ECC is attributed to a larger $J_b'/J_{tip}$ ratio.
- In general, the 100BCSA-55OA and 100BCSA-70OA mixtures demonstrate the best crack width control, meeting the criteria for optimal ECC performance by keeping crack widths below 100 μm. This ensures improved durability and resistance to aggressive exposure conditions. The 50PC/50BCSA-55OA mixture, despite its higher average crack width, could potentially benefit from better material optimization and fiber alignment to improve crack width control.
- The 100BCSA-55OA ECC mixture demonstrates excellent flexural performance with significant ductility and energy absorption capacity, as evidenced by its pseudo strain-hardening behavior, high flexural strength, and deflection-hardening characteristics. The material's ability to sustain multiple cracks while maintaining load-bearing capacity

highlights its superior toughness and deformation resistance compared to conventional concrete.

Conclusions from BCSA corrosion study:

- The rate of compressive strength should not be taken as analogous to the development of mixture density, improved durability, or corrosion protection.
- Lower w/cm mixtures have better corrosion protection performance across changes in cover depths, moist cure time, and silane surface treatment. Mixtures containing FA did not follow the same trend.
- Increasing cover depths was effective in extending the time in which it took for specimens to exceed the TC limit. The increased distance for chloride ions to travel before reaching reinforcing steel extended the time to corrosion.
- Increasing moist cure time was effective in extending the time in which it took for specimens to exceed the TC limit. Additional hydration products from the hydration of belite protects reinforcing steel from corrosion if enough curing time is provided.
- The combination of lower w/cm, increased cover depth, and increased moist cure time was effective in protecting reinforcing steel from corrosion. Silane surface treatments were the most effective form of corrosion protection.
- An exponential relationship between $f_c$-UPV exists but may be more accurate at earlier ages.

Overall, this research underscores the viability of BCSA cement as an effective substitute for PC in infrastructure applications including ECC or where corrosion performance is needed. BCSA can enhance both the use and mechanical performance of cementitious materials. Future studies are recommended to further investigate the effects of small and large percentages of PC replacement with BCSA cement on the tensile properties of ECCs. It is important to note that the documented results cover early to medium-term curing periods (1-28 days), and additional studies are needed to assess longer-term performance. While the corrosion performance of BCSA cement is not as strong as PC, mix design, curing, cover depth, and surface coatings are all levers which can be pulled to improve the corrosion performance of BCSA cement concrete to an acceptable level. Future research should investigate other mixture proportions and protective measures and should investigate the formation of hydration products at different ages and with different access to free water.

# Chapter 6. Implementation of Project Outputs

The implementation of the study outputs offers significant impacts and benefits for infrastructure repair. By replacing traditional Portland cement with BCSA cement for applications such as ECC, the study promotes the development of non-traditional construction materials. This material can improve the service life of infrastructure, reduce maintenance costs, and minimize impacts over time.

Status of Implementation

- Presentation (Lecture): American Concrete Institute Convention Spring 2024
  The study findings have been accepted for presentation at the American Concrete Institute Convention in Spring 2024, a prestigious platform for advancing concrete-related research. The lecture, titled *"Replacing Portland Cement in Engineered Cementitious Composites with Calcium Sulfoaluminate Cements for Infrastructure Repair"*, signifies growing industry interest and acceptance of CSA-based ECCs. This presentation enabled knowledge dissemination to researchers, engineers, and practitioners, fostering industry discussions on the feasibility and benefits of CSA cement for construction.
- Presentation (Poster): TRB Conference 2025
  The study has also been accepted for presentation at the Transportation Research Board Annual Meeting 2025 under the poster session *"TRBAM-25-04571: Investigating Belitic Calcium Sulfoaluminate Cement as Replacement for Portland Cement in Engineered Cementitious Composites"*. The TRB platform facilitates interactions with transportation professionals, policymakers, and researchers, providing opportunities to highlight the material's performance benefits and potential in transportation infrastructure repair. The poster presentation supports broader outreach and feedback, advancing the path toward real-world implementation.
- A paper is under preparation detailing the corrosion study reported here. This paper is targeted for submission to the journal *Construction and Building Materials*.

These presentations reflect growing recognition of the study's findings within professional and academic circles. The outputs are paving the way for further field testing, collaboration with industry stakeholders, and eventual adoption of CSA-based ECCs in infrastructure repair projects.

# Chapter 7. Technology Transfer and Community Engagement and Participation (CEP) Activities

As part of the technology transfer and CEP activities, the findings of this study are being integrated into practical educational initiatives to enhance understanding and promote adoption of advanced materials. In the Fall 2024 term, the CE 4660 *Infrastructure Condition Assessment* course included a laboratory practice focusing on Ultrasonic Testing Applications with BCSA-ECC mixtures. Specifically, students will conduct ultrasonic velocity tests, a non-destructive testing (NDT) method used to evaluate the material's density, homogeneity, and structural integrity by measuring the velocity of ultrasonic waves. This hands-on experience will enable students to assess the quality and performance of BCSA-based ECCs, particularly in identifying cracks, defects, and overall durability—critical aspects for infrastructure repair.

This laboratory activity provides significant benefits by bridging theoretical knowledge and practical skills. It introduces students to innovative cementitious materials, emphasizing the role of various solutions in infrastructure development. By learning advanced NDT techniques, students gain industry-relevant skills and exposure to real-world applications, strengthening their capabilities as future engineers and researchers. Furthermore, this activity encourages workforce development by equipping students with tools to evaluate and implement these materials in infrastructure repair. The laboratory practice also serves as a platform for broader community engagement, involving local agencies, researchers, and professionals through demonstrations and collaborative knowledge exchange. Overall, this initiative highlights the importance of ultrasonic testing and innovative materials like BCSA-ECCs in achieving long-term infrastructure solutions.

**Figure 43. 100BCSA-ECC being tested with ultrasonic velocity device.**

At UARK, the PI presented at a dinner hosted for the Engineering Career Awareness Program (ECAP). ECAP is a recruiting and support program for students in engineering which provides tools to help them succeed. This presentation covered the research in this report and was intended to expose potential future researchers to topics in concrete.

# Chapter 8. Invention Disclosures and Patents, Publications, Presentations, Reports, Project Website, and Social Media Listings

- Presentation (Lecture): American Concrete Institute Convention Spring 2024
  The study findings were presented at the American Concrete Institute Convention in Spring 2024, a prestigious platform for advancing concrete-related research. The lecture, titled *"Replacing Portland Cement in Engineered Cementitious Composites with Calcium Sulfoaluminate Cements for Infrastructure Repair."*
- Presentation (Poster): TRB Conference 2025
  The study was presented at the Transportation Research Board Annual Meeting 2025 under the poster session *"TRBAM-25-04571: Investigating Belitic Calcium Sulfoaluminate Cement as Replacement for Portland Cement in Engineered Cementitious Composites."*

# References


Acarturk, B. C. and Burris, L. E., Investigations of the Optimal Requirements for Curing of Calcium Sulfoaluminate Cement Systems, *CEMENT*, vol. **12**, p. 100072, accessed June 20, 2024, June 1, 2023. DOI: 10.1016/J.CEMENT.2023.100072

ACI Committee 228, ACI 228.1R-19 Report on Methods for Estimating In-Place Concrete Strength, American Concrete Institute, Farmington Hills, MI, 2019.

ACI Committee 318, Building Code Requirements for Structural Concrete : (ACI 318-19) ; and Commentary (ACI 318R-19), Farmington Hills, MI: American Concrete Institute, 2019.

Aïtcin, P. C., Portland Cement, in *Science and Technology of Concrete Admixtures*, Woodhead Publishing, accessed November 26, 2024, pp. 27–51, 2016.

Alapati, P., Moradllo, M. K., Berke, N., Ley, M. T. and Kurtis, K. E., Designing Corrosion Resistant Systems with Alternative Cementitious Materials, *Cement*, vol. **8**, p. 100029, June 2022. DOI: 10.1016/j.cement.2022.100029

Almutairi, A. L., Tayeh, B. A., Adesina, A., Isleem, H. F. and Zeyad, A. M., Potential Applications of Geopolymer Concrete in Construction: A Review, *Case Studies in Construction Materials*, vol. **15**, p. e00733, accessed January 23, 2024, December 1, 2021. DOI: 10.1016/J.CSCM.2021.E00733

Amran, Y. H. M., Alyousef, R., Alabduljabbar, H. and El-Zeadani, M., Clean Production and Properties of Geopolymer Concrete; A Review, *Journal of Cleaner Production*, vol. **251**, p. 119679, accessed January 23, 2024, April 1, 2020. DOI: 10.1016/J.JCLEPRO.2019.119679

Arce, G. A., Noorvand, H., Hassan, M. M., Rupnow, T. and Dhakal, N., Feasibility of Low Fiber Content PVA-ECC for Jointless Pavement Application, *Construction and Building Materials*, vol. **268**, January 25, 2021. DOI: 10.1016/j.conbuildmat.2020.121131

Arce, G., Noorvand, H., Hassan, M. and Rupnow, T., Evaluation of the Performance of Engineered Cementitious Composites (ECC) Produced from Local Materials, *International Congress on Polymers in Concrete (ICPIC 2018)*, pp. 181–86, accessed March 20, 2024, from https://link.springer.com/chapter/10.1007/978-3-319-78175-4_21, 2018. DOI: 10.1007/978-3-319-78175-4_21

Arce, G., Noorvand, H., Hassan, M., Rupnow, T. and Hungria, R., Cost-Effective ECC with Low Fiber Content for Pavement Application, *MATEC Web of Conferences*, vol. **271**, p. 07001, 2019. DOI: 10.1051/matecconf/201927107001

ASTM, C 150-24 Specification for Portland Cement, July 1, 2024a.

ASTM, C109/C109M Standard Test Method for Compressive Strength of Hydraulic Cement Mortars (Using 2-in. or [50-Mm] Cube Specimens), *American Society for Testing and Materials (ASTM)*, accessed November 12, 2021, from https://www.astm.org/DATABASE.CART/HISTORICAL/C109C109M-16A.htm, 2019.

ASTM, C191 Test Methods for Time of Setting of Hydraulic Cement by Vicat Needle, October 1, 2021.

ASTM, C219 Terminology Relating to Hydraulic and Other Inorganic Cements, April 1, 2024b.

ASTM, C230 Specification for Flow Table for Use in Tests of Hydraulic Cement, April 1, 2023.

ASTM, C1437 − 20 Test Method for Flow of Hydraulic Cement Mortar, 2020.

ASTM Standard C39/C39M-21, Standard Test Method for Compressive Strength of Cylindrical Concrete Specimens, *ASTM Standard C39-21*, ASTM International, West Conshohocken, PA, 2021.

ASTM Standard C138/C138M-24a, Standard Test Method for Density (Unit Weight), Yield, and Air Content (Gravimetric) of Concrete, ASTM International, West Conshohocken, PA, Jul. 1, 2024.

ASTM Standard C143/C143M-20, Standard Test Method for Slump of Hydraulic-Cement Concrete, *ASTM Standard C143-20*, ASTM International, West Conshohocken, PA, 2020.

ASTM Standard C192/C192M-19, Standard Practice for Making and Curing Concrete Test Specimens in the Laboratory, West Conshohocken, PA, 2019.

ASTM Standard C231/C231M-24, Standard Test Method for Air Content of Freshly Mixed Concrete by the Pressure Method, ASTM International, West Conshohocken, PA, Jan. 1, 2024.

ASTM Standard C597-22, Standard Test Method for Ultrasonic Pulse Velocity Through Concrete, *ASTM Standard C597-22*, ASTM International, West Conshohocken, PA, 2022.

ASTM Standard C881/C881-20a, Standard Specification for Epoxy-Resin-Base Bonding Systems for Concrete, ASTM International, West Conshohocken, PA, Oct. 1, 2020.

ASTM Standard G109-21, Standard Test Methods for Determining Effects of Chemical Admixtures on Corrosion of Embedded Steel Reinforcement in Concrete Exposed to Chloride Environments, *ASTM Standard G109-21*, ASTM International, West Conshohocken, PA, 2021.

Bescher, E. P., Ramseyer, C., Bescher, E. P., Kim, J., Ramseyer, C. and Vallens, J. K., Low Carbon Footprint Pavement: History of Use, Performance and New Opportunities for Belitic Calcium Sulfoaluminate, accessed January 25, 2024, from https://www.researchgate.net/publication/326300478, 2018.

Burris, L. E. and Kurtis, K. E., Water-to-Cement Ratio of Calcium Sulfoaluminate Belite Cements: Hydration, Setting Time, and Strength Development, *Cement*, vol. **8**, p. 100032, accessed June 20, 2024, June 1, 2022. DOI: 10.1016/J.CEMENT.2022.100032

Bye, G. C. ., Portland Cement : Composition, Production and Properties, p. 225, accessed November 26, 2024, from https://books.google.com/books/about/Portland_Cement.html?id=W8oYW15gH18C, 1999.

Cai, X., Yang, D., Zhang, D., Cui, J., Wang, W. and Liu, L., Development of High-Early-Strength Low-Carbon Engineered Cementitious Composites with Calcium Sulfoaluminate Cement Incorporating High-Volume Fly Ash, *Case Studies in*

*Construction Materials*, vol. **18**, p. e01959, accessed September 4, 2023, July 1, 2023. DOI: 10.1016/j.cscm.2023.e01959

Carsana, M., Canonico, F. and Bertolini, L., Corrosion Resistance of Steel Embedded in Sulfoaluminate-Based Binders, *Cement and Concrete Composites*, vol. **88**, pp. 211–19, April 1, 2018a. DOI: 10.1016/j.cemconcomp.2018.01.014

Carsana, M., Canonico, F. and Bertolini, L., Corrosion Resistance of Steel Embedded in Sulfoaluminate-Based Binders, *Cement and Concrete Composites*, vol. **88**, pp. 211–19, April 1, 2018b. DOI: 10.1016/j.cemconcomp.2018.01.014

Chen, I. A., Hargis, C. W. and Juenger, M. C. G., Understanding Expansion in Calcium Sulfoaluminate-Belite Cements, *Cement and Concrete Research*, vol. **42**, no. 1, pp. 51–60, accessed September 18, 2023, January 1, 2012. DOI: 10.1016/j.cemconres.2011.07.010

Cheriaf, M., Rocha, J. C. and Péra, J., Pozzolanic Properties of Pulverized Coal Combustion Bottom Ash, *Cement and Concrete Research*, vol. **29**, no. 9, pp. 1387–91, accessed July 17, 2024, September 1, 1999. DOI: 10.1016/S0008-8846(99)00098-8

Coppola, L., Beretta, S., Bignozzi, M. C., Bolzoni, F., Brenna, A., Cabrini, M., Candamano, S., et al., The Improvement of Durability of Reinforced Concretes for Sustainable Structures: A Review on Different Approaches, *Materials*, vol. **15**, no. 8, April 1, 2022. DOI: 10.3390/ma15082728

Coppola, L., Coffetti, D., Crotti, E., Dell'Aversano, R., Gazzaniga, G. and Pastore, T., Influence of Lithium Carbonate and Sodium Carbonate on Physical and Elastic Properties and on Carbonation Resistance of Calcium Sulphoaluminate-Based Mortars, *Applied Sciences (Switzerland)*, vol. **10**, no. 1, January 1, 2020. DOI: 10.3390/app10010176

Deo, O., Bhuskute, N., Paniagua, J., Guijosa, J., Rivera, J. and Bescher, E. P., A New Belitic Calcium Sulfoaluminate Cement, *Journal of Materials in Civil Engineering*, vol. **35**, no. 11, p. 04023422, accessed January 25, 2024, from https://ascelibrary.org/doi/abs/10.1061/JMCEE7.MTENG-15950, November 4, 2023. DOI: https://doi.org/10.1061/JMCEE7.MTENG-15950

Ding, Y., Yu, K. Q., Yu, J. tao and Xu, S. lang, Structural Behaviors of Ultra-High Performance Engineered Cementitious Composites (UHP-ECC) Beams Subjected to Bending-Experimental Study, *Construction and Building Materials*, vol. **177**, pp. 102–15, July 20, 2018. DOI: 10.1016/j.conbuildmat.2018.05.122

Ding, Y., Yu, K., and Li, M., A Review on High-Strength Engineered Cementitious Composites (HS-ECC): Design, Mechanical Property and Structural Application, *Structures*, January 1, 2022.

Duan, P., Chen, W., Ma, J. and Shui, Z., Influence of Layered Double Hydroxides on Microstructure and Carbonation Resistance of Sulphoaluminate Cement Concrete, *Construction and Building Materials*, vol. **48**, pp. 601–9, 2013. DOI: 10.1016/j.conbuildmat.2013.07.049

Fischer, G. and Li, V. C., Deformation Behavior of Fiber-Reinforced Polymer Reinforced Engineered Cementitious Composite (ECC) Flexural Members Under Reversed Cyclic Loading Conditions, *Aci Structural Journal*, vol. **100**, no. 1, pp. 25–35, accessed November 26, 2024, January 2003. DOI: 10.14359/12436

Game, D., Arce, G., Hassan, M. M., Noorvand, H., Subedi, S. and Rupnow, T., Development of Practical and Cost-Effective Ultra-High-Performance Engineered Cementitious Composites Using Natural Sand and No Silica Fume, in *Transportation Research Record*, SAGE Publications Ltd, pp. 312–28, 2022.

García-Maté, M., La Torre, A. G. De, León-Reina, L., Aranda, M. A. G. and Santacruz, I., Hydration Studies of Calcium Sulfoaluminate Cements Blended with Fly Ash, *Cement and Concrete Research*, vol. **54**, pp. 12–20, accessed June 26, 2024, December 1, 2013. DOI: 10.1016/J.CEMCONRES.2013.07.010

Gardner, D., Lark, R., Jefferson, T. and Davies, R., A Survey on Problems Encountered in Current Concrete Construction and the Potential Benefits of Self-Healing Cementitious Materials, *Case Studies in Construction Materials*, vol. **8**, pp. 238–47, accessed January 23, 2024, June 1, 2018. DOI: 10.1016/J.CSCM.2018.02.002

Gastaldi, D., Bertola, F., Canonico, F., Buzzi, L., Mutke, S., Irico, S., Paul, G., Marchese, L. and Boccaleri, E., A Chemical/Mineralogical Investigation of the Behavior of Sulfoaluminate Binders Submitted to Accelerated Carbonation, *Cement and Concrete Research*, vol. **109**, pp. 30–41, July 1, 2018. DOI: 10.1016/j.cemconres.2018.04.006

Gou, H., Zhang, Z., Zhu, M., Zhu, H., Mendis, P. and Sofi, M., Sustainable Engineered Cementitious Composites Featuring High Belite-Calcium Sulfoaluminate Cement and Gypsum, *SSRN* , accessed July 29, 2024, from https://papers.ssrn.com/abstract=4791969, 2024. DOI: 10.2139/SSRN.4791969

Jiang, B., Qian, Z., Gu, D. and Pan, J., Repair Concrete Structures with High-Early-Strength Engineered Cementitious Composites (HES-ECC): Material Design and Interfacial Behavior, *Journal of Building Engineering*, vol. **68**, p. 106060, accessed February 1, 2024, June 1, 2023. DOI: 10.1016/J.JOBE.2023.106060

JSCE, Recommendations for Design and Construction of High Performance Fiber Reinforced Cement Composites with Multiple Fine Cracks (HPFRCC), Mar. 2008.

Kameswara Rao, B., Achyutha Kumar Reddy, M. and Venkateswara Rao, A., Effect of Flyash as Cement Replacement Material and Pore Filling Material in Concrete, *Materials Today: Proceedings*, vol. **52**, pp. 1775–80, accessed November 29, 2024, January 1, 2022. DOI: 10.1016/J.MATPR.2021.11.444

Kanda, T., and Li, V. C., Practical Design Criteria for Saturated Pseudo Strain Hardening Behavior in ECC, *Journal of Advanced Concrete Technology*, 2006.

LaDOTD, Standard Specifications for Roads and Bridges Manual, 2016.

Lewis, R. and Fidjestøl, P., *Lea's Chemistry of Cement and Concrete*, *Lea's Chemistry of Cement and Concrete*, Elsevier, accessed November 26, 2024, from https://books.google.com/books/about/Lea_s_Chemistry_of_Cement_and_Concrete.html?id=bpmLDwAAQBAJ, pp. 509–535, 2003.

Li, V. C., Engineered Cementitious Composites (ECC): Bendable Concrete for Sustainable and Resilient Infrastructure, Engineered Cementitious Composites (ECC): Bendable Concrete for Sustainable and Resilient Infrastructure, Springer Berlin Heidelberg, 2019.

Li, V. C., Engineered Cementitious Composites (ECC) Bendable Concrete for Sustainable and Resilient Infrastructure, n.d.

Luo, S., Bai, T., Guo, M., Wei, Y. and Ma, W., Impact of Freeze–Thaw Cycles on the Long-Term Performance of Concrete Pavement and Related Improvement Measures: A Review, *Materials 2022, Vol. 15, Page 4568*, vol. **15**, no. 13, p. 4568, accessed November 26, 2024, from https://www.mdpi.com/1996-1944/15/13/4568/htm, June 29, 2022. DOI: 10.3390/MA15134568

Lv, L., Hong, X., Ding, Z., Ma, X. and Li, H., Preparation and Characterization of Calcium Sulfoaluminate Based Engineered Cementitious Composites for Rapid Repairing of Concrete Member, *Frontiers in Materials*, vol. **7**, p. 575468, accessed September 18, 2023, from https://www.frontiersin.org/article/10.3389/fmats.2020.00282/full, September 11, 2020. DOI: 10.3389/fmats.2020.00282

Maaddawy, T. El, Soudki, K. and Topper, T., Long-Term Performance of Corrosion-Damaged Reinforced Concrete Beams, *Aci Structural Journal*, vol. **102**, no. 5, pp. 649–56, accessed November 26, 2024, September 2005. DOI: 10.14359/14660

Marsh, A. T. M., Velenturf, A. P. M. and Bernal, S. A., Circular Economy Strategies for Concrete: Implementation and Integration, *Journal of Cleaner Production*, vol. **362**, p. 132486, accessed October 11, 2023, August 15, 2022. DOI: 10.1016/J.JCLEPRO.2022.132486

Mehta, P. K., and Gerwick, B. C., CRACKING-CORROSION INTERACTION IN CONCRETE EXPOSED TO MARINE ENVIRONMENT., *Concrete International*, vol. **4**, no. 10, 1982.

Mehta, P. K. and Monteiro, P. J. M., *Concrete: Microstructure, Properties, and Materials*, McGraw-Hill, 2006.

Mindess, S., Developments in the Formulation and Reinforcement of Concrete, Woodhead Publishing, 2019.

Mohammed, T. U. and Rahman, M. N., Effect of Types of Aggregate and Sand-to-Aggregate Volume Ratio on UPV in Concrete, *Construction and Building Materials*, vol. **125**, pp. 832–41, October 30, 2016. DOI: 10.1016/j.conbuildmat.2016.08.102

Napp, T. A., Gambhir, A., Hills, T. P., Florin, N. and Fennell, P. S., A Review of the Technologies, Economics and Policy Instruments for Decarbonising Energy-Intensive Manufacturing Industries, *Renewable and Sustainable Energy Reviews*, vol. **30**, pp. 616–40, accessed January 23, 2024, February 1, 2014. DOI: 10.1016/J.RSER.2013.10.036

Noorvand, H., Arce, G. A. and Hassan, M. M., Evaluation of the Effects of Engineered Cementitious Composites (ECC) Plasticity on Concrete Pavement Performance, *International Journal of Pavement Engineering*, vol. **23**, no. 13, pp. 4474–86, accessed July 26, 2024, from https://www.tandfonline.com/doi/abs/10.1080/10298436.2021.1954180, November 10, 2022. DOI: 10.1080/10298436.2021.1954180

Noorvand, H., Arce, G., Hassan, M., Rupnow, T. and Mohammad, L. N., Investigation of the Mechanical Properties of Engineered Cementitious Composites with Low Fiber Content and with Crumb Rubber and High Fly Ash Content, *Transportation Research Record*, vol. **2673**, no. 5, pp. 418–28, May 1, 2019. DOI: 10.1177/0361198119837510

Olsson, J. A., Miller, S. A. and Alexander, M. G., Near-Term Pathways for Decarbonizing Global Concrete Production, *Nature Communications*, vol. **14**, no. 1, accessed

October 11, 2023, from /pmc/articles/PMC10387082/, December 1, 2023. DOI: 10.1038/S41467-023-40302-0

O'Reilly, M., Farshadfar, O. and Darwin, D., Effect of Supplementary Cementitious Materials on Chloride Threshold and Corrosion Rate of Reinforcement, *ACI Materials Journal*, vol. **116**, no. 1, pp. 125–33, 2019. DOI: 10.14359/51710968

Quillin, K., Performance of Belite-Sulfoaluminate Cements, *Cement and Concrete Research*, vol. **31**, pp. 1341–49, 2001.

S, A. V. and S, R. K. M., Review on the Mechanism and Mitigation of Cracks in Concrete, *Applications in Engineering Science*, vol. **16**, p. 100154, accessed November 26, 2024, December 1, 2023. DOI: 10.1016/J.APPLES.2023.100154

Şahmaran, M., Al-Emam, M., Yıldırım, G., Şimşek, Y. E., Erdem, T. K. and Lachemi, M., High-Early-Strength Ductile Cementitious Composites with Characteristics of Low Early-Age Shrinkage for Repair of Infrastructures, *Materials and Structures/Materiaux et Constructions*, vol. **48**, no. 5, pp. 1389–1403, accessed March 1, 2024, from https://link.springer.com/article/10.1617/s11527-013-0241-z, May 1, 2015. DOI: 10.1617/S11527-013-0241-Z/TABLES/2

Savadogo, N., Traoré, Y. B., Nshimiyimana, P., Messan, A., Hannawi, K., Tsobnang, F. and Prince Agbodjan, W., Hydration and Physico-Mechanical Characterization of Bottom Ash-Based Cement, *Construction and Building Materials*, vol. **434**, p. 136679, accessed July 13, 2024, July 5, 2024. DOI: 10.1016/J.CONBUILDMAT.2024.136679

Shumuye, E. D., Li, W., Fang, G., Wang, Z., Liu, J. and Zerfu, K., Review on the Durability of Eco-Friendly Engineering Cementitious Composite (ECC), *Case Studies in Construction Materials*, vol. **19**, p. e02324, accessed February 6, 2024, December 1, 2023. DOI: 10.1016/J.CSCM.2023.E02324

Subedi, S., Arce, G. A., Hassan, M. M., Barbato, M. and Mohammad, L. N., Effect of Raw Sugarcane Bagasse Ash as Sand Replacement on the Fiber-Bridging Properties of Engineered Cementitious Composites, in *Transportation Research Record*, SAGE Publications Ltd, pp. 1028–42, 2021.

Winnefeld, F. and Lothenbach, B., Hydration of Calcium Sulfoaluminate Cements - Experimental Findings and Thermodynamic Modelling, *Cement and Concrete Research*, vol. **40**, no. 8, pp. 1239–47, accessed September 18, 2023, August 1, 2010. DOI: 10.1016/j.cemconres.2009.08.014

Xie, W., Xu, X., Xu, C., Tian, F., Mao, Q., Li, H., Liu, L. and Qin, G., An Experimental Study and Axial Tensile Constitutive Model of the Toughness of PP-SACC for Rapid Repairs, *Frontiers in Built Environment*, vol. **9**, p. 1137569, accessed February 10, 2024, May 4, 2023. DOI: 10.3389/FBUIL.2023.1137569/BIBTEX

Yoon, H. N., Seo, J., Kim, S., Lee, H. K. and Park, S., Hydration of Calcium Sulfoaluminate Cement Blended with Blast-Furnace Slag, *Construction and Building Materials*, vol. **268**, p. 121214, accessed July 12, 2024, January 25, 2021. DOI: 10.1016/J.CONBUILDMAT.2020.121214

Zhang, L. and Glasser, F. P., Investigation of the Microstructure and Carbonation of C$\bar{S}$A-Based Concretes Removed from Service, *Cement and Concrete Research*, vol. **35**, no. 12, pp. 2252–60, December 2005. DOI: 10.1016/j.cemconres.2004.08.007

Zhou, J., Ye, G. and Breugel, K. van, Cement Hydration and Microstructure in Concrete Repairs with Cementitious Repair Materials, *Construction and Building Materials*, vol.

**112**, pp. 765–72, accessed January 20, 2024, June 1, 2016. DOI: 10.1016/J.CONBUILDMAT.2016.02.203

Zivica, V., Palou, M. T. and Bágeľ, T. I. Ľ., High Strength Metahalloysite Based Geopolymer, *Composites Part B: Engineering*, vol. **57**, pp. 155–65, 2014. DOI: 10.1016/j.compositesb.2013.09.034

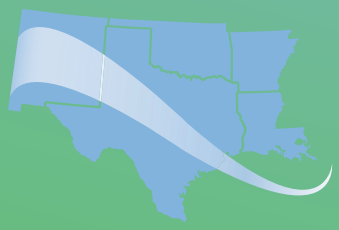

SOUTHERN PLAINS
TRANSPORTATION CENTER

The University of Oklahoma | OU Gallogly College of Engineering
202 W Boyd St, Room 213A, Norman, OK 73019 | (405) 325-4682 | Email: sptc@ou.edu